Simplex Simulated Annealing, a Hybrid Approach to Geoacoustic Inversion with Application to Mediterranean Sea Acoustic Data

by

Mark Ryan Fallat
B.Sc., University of Victoria, 1997

A Thesis submitted in Partial Fulfillment of the
Requirements for the Degree of

MASTER OF SCIENCE

in the

SCHOOL OF EARTH AND OCEAN SCIENCE

We accept this thesis as conforming
to the required standard

[redacted]

Dr. S.E. Dosso, Supervisor (School of Earth and Ocean Science)

[redacted]

Dr. N.R. Chapman, Departmental Member (School of Earth and Ocean Science)

[redacted]

Dr. R. L. Kirlin, Outside Member (Department of Electrical Engineering)

[redacted]

Dr. A. Antoniou, External Examiner (Department of Electrical Engineering,)

Supervisor: Dr. S.E. Dosso

Abstract

Recently, in ocean acoustics, there has been a great deal of interest in the development of inversion algorithms. One problem these algorithms have been applied to is geoacoustic inversion. In geoacoustic inversion, properties of the seabed are sought from measurements of acoustic energy that has propagated through the ocean environment. In this thesis, a new hybrid algorithm, simplex simulated annealing, is developed for the geoacoustic inversion problem. Simplex simulated annealing is a combination of the local downhill simplex method and a fast simulated annealing global search algorithm. Hybrid algorithms are effective and efficient because they exploit the good features of the local and global algorithms while overcoming the respective weaknesses of the techniques. The simplex simulated annealing algorithm is validated using synthetic testcases and is compared with both downhill simplex and simulated annealing. The new algorithm is also applied to experimental data recorded in the Mediterranean Sea. For the experimental inversion the results are in good agreement with the available ground truth data and results from previous experiments conducted in the same region.

Examiners:

Dr. S.E. Dosso, Supervisor (School of Earth and Ocean Science)

Dr. N.R. Chapman, Departmental Member (School of Earth and Ocean Science)

Dr. R. L. Kirlin, Outside Member (Department of Electrical Engineering).

Dr. A. Antoniou, External Examiner (Department of Electrical Engineering,)

Table of Contents

List of Tables

List of Figures

Acknowledgments

I would like to thank my supervisor Dr. Stan Dosso for his endless support and extremely valuable guidance. Over the past three years Stan has offered nothing but encouragement and has been very patient with me (and my ideas). Thanks Stan, a lot of my success is because of you. I would also like to thank the members, past and present, of the Ocean Acoustics Group at the University of Victoria for the valuable discussions we had (even if they weren't always about acoustics). I would like to extend a special thanks to SACLANT Centre for the Summer Research Assistant position that made some of this work possible. I would also like to thank Peter Nielsen and Martin Siderius for their help during my time at SACLANTCEN. It goes without saying that, I thank all my family and friends (thanks for the useful comments Peter) for always being there and never letting me falter. I'm stronger because of all of you. Finally, I would like to thank Jamie Vala. This is for you, you knew I could do it.

Chapter 1

Introduction

In order to properly model acoustic propagation in an ocean environment, one must have a knowledge of the geoacoustic properties of the environment. This is especially true for shallow water propagation where there is a great deal of acoustic interaction with the seafloor. However, these properties are typically difficult and expensive to measure *in situ*. Therefore, inverse methods are often applied to estimates geoacoustic properties in a cost-effective matter.

The problem of determining seabed properties can be broken into two parts, the first part is the actual experiment where acoustic fields are recorded at an array of hydrophones. The second part is the geoacoustic inversion which involves several steps. First, a geoacoustic model must be parameterized for the problem. This is a discrete model of unknown parameters defined by $\mathbf{m}= \{m_i, i = 1, ..., M\}$. For each unknown parameter, a search interval of physically meaningful values must be defined. All available *a priori* information (e.g., CTD casts, echosounder data, core samples, etc.) should be built into the inverse problem through the model parameterization and choice of model limits. A forward model must then be chosen which simulates acoustic propagation in the particular ocean environment. An inversion can then be carried out to minimize an objective or cost function which represents the mismatch between the measured and replica data.

The goal of the inversion is to determine the set of model parameters which minimizes the mismatch. This can be a challenging problem due to the size of the parameter space, which increases geometrically with the number of parameters, and the presence of local minima due to the nonlinearity of the inverse problem.

A number of different algorithms have been applied to the geoacoustic inversion

problem. The different algorithms can be classified as local, global and hybrid methods. Local methods are sensitive to local gradients in the objective function and can move effectively downhill, but typically become trapped in a local minimum near the staring model. A variety of local algorithms exist including the Gauss-Newton method (Gerstoft 1995), the conjugate gradient method (Chunduru *et al.* 1997) and the downhill simplex method (Nelder and Mead 1965; Press *et al.* 1992). Rajan *et al.* (1987) and Zala and Ozard (1998) have both successfully applied local methods to the geoacoustic inversion problem.

Global inversion methods are designed to widely search the parameter space by using a random process to repeatedly perturb the model, and include the ability to move uphill in the objective function to escape local minima. However, since model perturbations are computed randomly (without gradient information), global methods are inefficient at moving downhill and can be computationally expensive. Algorithms such as simulated annealing (Collins *et al.* 1992; Lane 1992; Dosso *et al.* 1993; Lindsay and Chapman 1993; Collins and Fishman 1995; Fallat and Dosso 1998) and genetic algorithms (Gerstoft 1994; Gerstoft 1995; Hermand and Gerstoft 1996) are the most extensively employed techniques for geoacoustic inversion.

Hybrid methods combine local and global inversions in an attempt to retain the advantages of each while overcoming their respective weaknesses. Hybrid methods have the potential to move effectively downhill, yet avoid becoming trapped in local minima, and lead to a solution that is independent of the starting model. Several different hybrid techniques have been developed. These include a Gauss-Newton, genetic algorithm hybrid (Gerstoft 1995), a conjugate gradient, simulated annealing combination (Chunduru *et al.* 1997) and downhill simplex, simulated annealing variations (Press *et al.* 1992; Liu *et al.* 1995).

Determining an appropriate inversion method for a particular problem can be difficult. Hybrid methods would seem to be the best choice as they retain the good features of their respective local and global methods. The goal of this thesis is to

develop a new hybrid algorithm for solving the geoacoustic inversion problem. Here, the simplex simulated annealing algorithm, which combines the downhill simplex method and simulated annealing, is developed. The algorithm is validated using noise-free synthetic testcases from a geoacoustic inversion workshop (Tolstoy *et al.* 1998) and compared with both downhill simplex and simulated annealing. Simplex simulated annealing was also applied to experimental data to produce estimates of geoacoustic and geometric properties. The PROSIM'97 experiment (Nielsen *et al.* 1998) was conducted off the west coast of Italy. During the experiment environmental and acoustic data were recorded from a well known area of the Mediterranean Sea.

Chapter 2 of this thesis provides a brief background to the geoacoustic inverse problem. It includes a simple discussion of general inverse theory, a description of geoacoustic inversion and matched field processing, and an explanation of the numerical models employed. In Chapter 3, the simplex simulated annealing algorithm is described along with the downhill simplex method and simulated annealing. Chapter 4 describes the synthetic-data inversions used to validate simplex simulated annealing and the comparison with the other algorithms. In Chapter 5 simplex simulated annealing is used to invert the experimental data from the Mediterranean Sea. This includes a description of the experiment and the inversion results as well as a comparison with past inversion experiments. Finally, the conclusions of this work are given in Chapter 6.

Chapter 2

Geoacoustic Inversion

Inverse theory can be defined as:

> *The estimation of parameters of a postulated model*
> *for some physical system from a set of observations*
> *of some process which interacts with the system.*

This chapter provides a general background to geoacoustic inversion. It starts with a basic introduction to general inverse theory. This is followed by a brief description of geoacoustic inversion and one of the techniques, matched field processing, that is applied to this problem. The final section provides a brief overview of numerical propagation models with particular attention paid to the model (normal modes) used in this thesis. This chapter is designed to give an idea of the basic problem; for more information the reader should look to the following references: for inverse theory, Menke (1984), Tarantola (1987), Press *et al.* (1992), Sen and Stoffa (1995); for geoacoustic inversion, Collins *et al.* (1992), Dosso *et al.* (1993), Gerstoft (1994) and for numerical modeling, Jensen *et al.* (1994).

2.1 The Inverse Problem

To properly understand the inverse problem, one must first have an understanding of the forward problem. The forward problem ($\mathbf{F}$) can be described as: given some model $\mathbf{m}$ of the physical system, compute the data $\mathbf{d}$ that will be observed, i.e.,

$$\mathbf{F}[\mathbf{m}] = \mathbf{d}. \tag{2.1}$$

If a satisfactory solution to the forward model can not be found then there is no reason to even consider the inverse problem.

The inverse problem ($\mathbf{F^{-1}}$) can be described as: given a set of data $\mathbf{d}$, determine the model $\mathbf{m}$ that gave rise to the data, i.e.,

$$\mathbf{m} = \mathbf{F}^{-1}[\mathbf{d}]. \tag{2.2}$$

Generally, the forward problem yields a solution that is unique and stable. The same statement is not true for the inverse problem. For the inverse problem there are two scenarios, first the data are complete and exact (represents an idealization), then the solution can be unique. Secondly, the data are incomplete and/or inexact (represents the real world); in this case the solution, if it exists at all, is non-unique and is often unstable. To overcome the stability and uniqueness issues associated with the inverse problem, some form of *a priori* information can be built into the problem.

Inverse problems are found in a wide range of physical sciences including astrophysics, geophysics, oceanography, and medical sciences to name a few. In ocean acoustics, one such inverse problem that has received a lot of attention is geoacoustic inversion.

2.2 Geoacoustic Inverse Problem

The propagation of acoustic energy in the ocean is influenced by both the ocean and seafloor properties. As the acoustic energy propagates through the ocean it can be described by a pressure disturbance p that satisfies the acoustic wave equation

$$\rho \nabla \cdot \left(\frac{1}{\rho} \nabla p \right) - \frac{1}{c^2} \frac{\partial^2 p}{\partial t^2} = 0, \tag{2.3}$$

where c is the sound speed and ρ is the density. When this energy comes in contact with an elastic medium (e.g., the seafloor) the environment supports both shear and

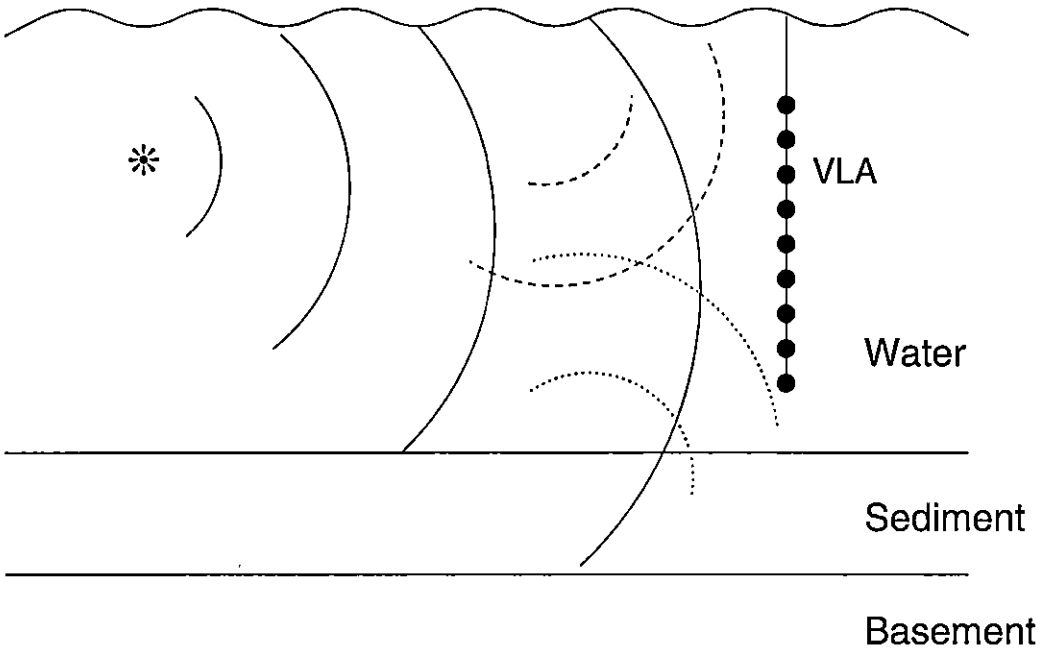

Figure 2.1 A simple schematic of how acoustic energy that propagates through the ocean environment interacts with the seafloor. The vertical line array (VLA) of sensors is were the acoustic energy is received.

compressional waves. Figure 2.1 is a simple schematic diagram demonstrating how the acoustic energy interacts with the ocean environment for a shallow water short range scenario.

To create a complete geoacoustic model, properties such as compressional speed c_p, shear speed c_s, compressional-wave attenuation α_p, shear-wave attenuation α_s, and the density ρ must be included. In particular, a knowledge of the variation of these properties over both range and depth may be required. The goal in geoacoustic inversion is to obtain estimates of the geoacoustic properties from measurements of the acoustic energy that has propagated through the particular ocean environment.

The parameterization of the geoacoustic model is one of the most important aspects of geoacoustic inversion. In general, the true form of the model is unknown, and must be either assumed or is included as part of the inversion. For simple problems,

the form of the model can be assumed to be a finite number of sediment layers over a semi-infinite basement. If the problem is more difficult and the form of the model must be included as part of the inversion there are two approaches that are typically employed. Both cases are based on seeking as simple a solution as possible (i.e., minimum-structure model). The first technique is an under-parameterized approach, where the inversion is successively repeated for an increasing number of model parameters (e.g., the number of layers). The other approach is to over-parameterize the model, but to include an explicit penalty for model structure in the objective function.

2.3 Matched Field Inversion

In recent years, matched field processing (MFP) has become a standard technique for geoacoustic inversion (Collins *et al.* 1992; Dosso *et al.* 1993; Lindsay and Chapman 1993; Collins and Fishman 1995; Fallat and Dosso 1998; Musil 1998; Fallat and Dosso 1999a; Fallat *et al.* 1999b). In principle, MFP is quite a simple technique (Tolstoy 1993) defined as a forward modeling approach to inversion. The problem starts with measurements of the ocean acoustic fields at an array of $N > 1$ sensors or hydrophones (e.g., Fig. 2.1 for a vertical line array (VLA) of sensors). A numerical propagation model is then used to simulate acoustic propagation in the ocean environment for different sets of model parameters. The goal is to determine the geoacoustic model parameters that minimize some measure of the mismatch between the measured and modeled acoustic fields. Therefore the MFP problem can essentially be defined as a global optimization.

In general, MFP is a difficult non-linear problem. The parameter space can be very large (possibly > 50 dimensions or unknowns see Dosso *et al.* 1993) and can have a large number of local minima. Other features that make the problem difficult are

correlations between parameters which lead to narrow oblique valleys in the parameter space, and the sensitivity of the data to various parameters which can vary over orders of magnitude.

The measure of mismatch between the measured and modeled fields can be defined in several different ways. Some of the most widely used measures include the Bartlett or linear processor, the minimum-variance processor, and the multiple constraint processor. For a detailed description of these and other processors the reader is recommend to Tolstoy (1993). In ocean acoustics, the Bartlett processor is by far the most popular measure of the mismatch as a direct result of its robustness.

In this thesis, the Bartlett processor was employed for the inversions. The form used here is given by

$$E(\mathbf{m}) = 1 - \frac{1}{F}\sum_{j=1}^{F}\frac{|\mathbf{p}(f_j)\cdot\mathbf{p}^*(\mathbf{m},f_j)|^2}{|\mathbf{p}(f_j)|^2|\mathbf{p}(\mathbf{m},f_j)|^2}, \tag{2.4}$$

where $F \geq 1$ is the number of frequency bands, $\mathbf{p}(f_j)$ is a vector of the acoustic pressure measured at an array, and $\mathbf{p}(\mathbf{m},f_j)$ is the modeled acoustic pressure for the model $\mathbf{m}$ at the frequency f_j. The pressures are summed coherently in depth and incoherently in frequency. With this definition, the mismatch has a value $E \in [0,1]$, with zero indicating a perfect match.

As stated earlier, MFP is a forward modeling approach to inversion. Therefore, one of the important steps for this problem is choosing an appropriate forward model. The next section describes the forward models used in the work.

2.4 Forward Models

Forward modeling is a numerical approach to solving the acoustic propagation problem. There are essentially five types of forward models:

- Normal modes,
- Ray theory,
- Parabolic equations,
- Wavenumber integrations methods,
- Finite difference and finite element methods.

A numerical model based on normal modes was used in this thesis. This model was chosen because it provides accurate estimates of the acoustic fields for range-independent and moderately range-dependent environments with a minimal amount of computation time. What follows is a brief overview of a normal mode model. Jensen *et al.* (1994) offers a detailed description of all of the different numerical models.

Normal mode methods are derived from the wave or Helmholtz equation (shown here in homogeneous form)

$$\frac{1}{r}\frac{\partial}{\partial r}\left(r\frac{\partial p}{\partial r}\right)+\rho\frac{\partial}{\partial z}\left(\frac{1}{\rho}\frac{\partial p}{\partial z}\right)+\frac{\omega^2}{c^2}p=0. \tag{2.5}$$

A solution is sought using the method of *separation of variables* in the form $p(r,z)=\Phi(r)\Psi(z)$. Substituting this into Eq. 2.5 and solving for a separation constant of $-k_{rm}^2$, two equations are obtained

$$\text{Radial}: \quad \frac{1}{r}\frac{d}{dr}\left(\frac{1}{r}\frac{d\Phi_m}{dr}\right)+k_{rm}^2\Phi_m=0 \tag{2.6}$$

$$\text{Depth}: \quad \rho\frac{d}{dz}\left(\frac{1}{\rho}\frac{d\Psi_m}{dz}\right)+\left(\frac{\omega^2}{c^2}-k_{rm}^2\right)=0. \tag{2.7}$$

The eigenfunctions of the depth equation are the normal modes. The eigenvalues of the radial equation are the radial wavenumbers. Using this approach the acoustic pressure can now be expressed as

$$p(r,z) = \sum_{m=1}^{\infty} \Phi_m(r)\Psi_m(z). \tag{2.8}$$

The eigenfunctions $\Phi_m(r)$ consist of Hankel functions, which substituted into Eq. 2.8 results in

$$p(r,z) = \frac{i}{4\rho(z_s)} \sum_{m=1}^{\infty} \Psi_m(z_s)\Psi_m(z)H_o^{(1)}(k_{rm}r). \tag{2.9}$$

Adopting the asymptotic approximation to the Hankel function for $k_{rm}r \gg 1$, produces the farfield solution given by

$$p(r,z) \simeq \frac{i}{\rho(z_s)\sqrt{8\pi r}} \exp(-i\pi/4) \sum_{m=1}^{\infty} \Psi_m(z_s)\Psi_m(z)\frac{\exp(ik_{rm}r)}{\sqrt{k_{rm}}}. \tag{2.10}$$

The normal mode codes ORCA (Westwood *et al.* 1996) and PROSIM (Nielsen *et al.* 1999) are used in this thesis. ORCA provides an efficient far-field solution to the (elastic) wave equation. PROSIM is a range-dependent version of the ORCA model. The range dependence was built in using the adiabatic approximation (Pierce 1965; Jensen *et al.* 1994) given by

$$p(r,z) \simeq \frac{i}{\rho(z_s)\sqrt{8\pi r}} \exp(-i\pi/4) \sum_{m=1}^{\infty} \Psi_m(z_s)\Psi_m(r,z)\frac{\exp(i\int_0^r k_{rm}(r')dr')}{\sqrt{k_{rm}(r)}}, \tag{2.11}$$

where $\Psi_m(z_s)$ are the mode functions calculated at the source and $\Psi_m(r,z)$ are the mode functions calculated at a range r. The adiabatic approximation assumes that there is no energy transfer between modes in going from one range to the next. To apply this approximation, the environment is divided into a discrete number of range segments. Each segment is taken to be range-independent. The wavenumbers

are computed for the individual segments and the range-dependent environment is constructed by joining the segments. This approximation is only valid for weakly range-dependent environments (e.g., a sloping bottom of $\approx 0.5°$) but the advantage is that it is computationally fast compared to coupled mode models.

Another important feature of PROSIM is that it only uses the real wavenumber axis to compute the fields. Normal mode models must search a wavenumber space to find the appropriate solutions. If shear properties or attenuations are included this search must be conducted in the complex plane and can therefore be computationally expensive. Therefore, in an attempt to conserve time the imaginary parts of the wavenumbers are ignored and the search is carried out only along the real axis. A perturbation method is used to model acoustic propagation with shear properties or attenuations when only the real wavenumbers are used. It should be noted that using only the real wavenumber axis is also an option in the standard ORCA model.

The wavenumber integration model SAFARI (Schmidt 1988) was indirectly used in this thesis. Synthetic testcases were generated using SAFARI and were obtained by the author for analysis. Wavenumber integration methods can also be applied to numerically solve the wave equation, but instead of using separation of variables, they numerically integrate the Helmholtz Green's function. This theory gives potentially exact solutions for all frequencies. Wavenumber integral methods can accurately model the nearfield and they can accurately include the effects of elastic media. The drawbacks are that they can only solve the range-independent problem and they can be computationally very slow.

Chapter 3

Inversion Algorithm

In this chapter the hybrid inversion algorithm, simplex simulated annealing (SSA), is developed. This algorithm combines the local downhill simplex method (DHS), and the global optimization simulated annealing (SA). The first section defines local methods and describes the DHS method. The next section describes global methods and gives an overview of SA. The final section describes the hybrid SSA algorithm with an explanation of how it overcomes the problems associated with local and global techniques.

3.1 The Downhill Simplex Method

Local optimization methods are based on iteratively improving a starting model by moving down the local gradient of the objective function. Since gradient information is used, these methods move effectively downhill, but typically become trapped in the closest local minimum. There are many different local methods including the Gauss-Newton method, conjugate gradient method, and the DHS method which is employed here.

The DHS method is based on an intuitive geometric scheme for moving downhill in the parameter space (Nelder and Mead 1965; Press *et al.* 1992). Although DHS is not necessarily the most efficient method of finding local minima, it does not require the computation of partial derivatives or the solving of systems of equations, and therefore each iteration is quite simple and efficient to compute.

The algorithm operates on a simplex of $M+1$ models in an M-dimensional space

(e.g., Fig. 3.1 a, for $M = 3$). The initial simplex can be chosen randomly from the parameter space. In order to move downhill, the simplex undergoes a series of transformations. Each model in the simplex is first ranked according to its mismatch E. The algorithm initially attempts to improve the model with the highest mismatch by reflecting it through the centroid of the simplex face containing the lowest-mismatch model as shown in Fig. 3.1 (b). If the new model has the lowest mismatch in the simplex, then an extension by a factor of two in the same direction is attempted (Fig. 3.1 c). If the reflection results in a model that still has the highest mismatch, the reflection is rejected and a contraction by a factor of two toward the face containing the lowest-mismatch model is carried out (Fig. 3.1 d). If none of these steps decrease E, then a multiple contraction by a factor of two in all dimensions, along the edges of the simplex, toward the lowest-mismatch model is performed (Fig. 3.1 e). If any of these steps result in a parameter value that is outside the given search bound, the parameter is set to the value of the nearest bound. This process is repeated until the difference between the highest- and lowest-mismatch models relative to their average is less than some tolerance ε, i.e.,

$$\frac{E_{\text{high}} - E_{\text{low}}}{(E_{\text{high}} + E_{\text{low}})/2} < \varepsilon, \tag{3.1}$$

or until a maximum number of iterations is reached.

3.2 Simulated Annealing

Global optimizations use random processes to repeatedly perturb model parameters in order to widely search the parameter space. These algorithms include the ability to move uphill in parameter space and therefore can escape local minima. Global methods require only computation of the objective function, not its derivatives, and are relatively insensitive to the starting model. The major drawback of

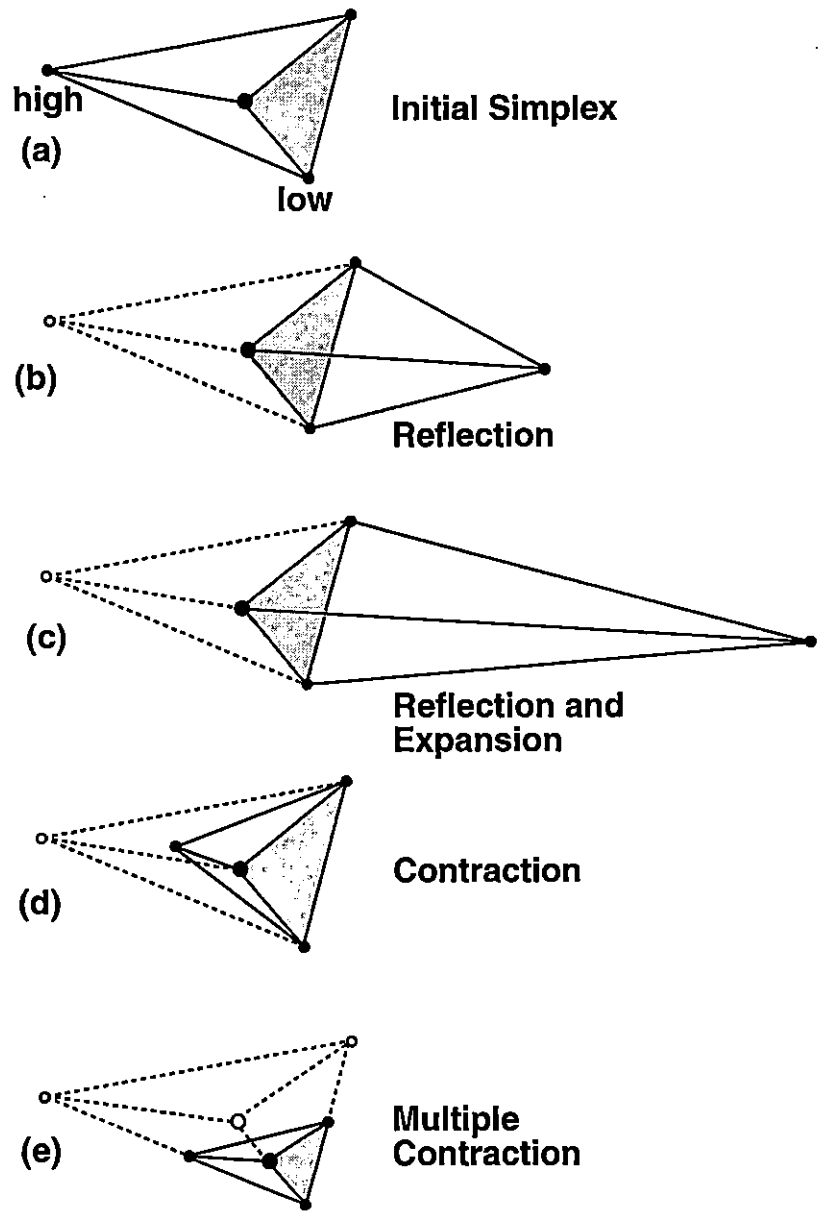

Figure 3.1 The types of steps attempted by the DHS algorithm in three dimensions after (after Press *et al.* 1992).

these methods is that since random perturbations, with no gradient information, are used they can be inefficient at moving downhill and can be computationally expensive. The two most popular global optimization algorithms are genetic algorithms (GA) (e.g., Gerstoft 1994; Gerstoft 1995; Hermand and Gerstoft 1996) and SA (e.g., Collins *et al.* 1992; Dosso *et al.* 1993; Lindsay and Chapman 1993; Collins and Fishman 1995; Fallat and Dosso 1998). In this section a fast SA algorithm is described.

SA is an optimization technique which is based on an analogy to the physical process of growing crystals by thermodynamic annealing (Kirkpatrick *et al.* 1983). It consists of a series of iterations involving random perturbations of the unknown parameters of a single starting model. Perturbations which decrease the mismatch are always accepted; perturbations which lead to an increase in mismatch are accepted conditionally, with a probability P that decreases with T according to the Boltzmann distribution

$$P(\Delta E) = \exp(-\Delta E/T). \tag{3.2}$$

Accepting some perturbations which increase the mismatch allows the algorithm to escape from local minima in search of a better solution. After each iteration a control parameter, the temperature T, is decreased slightly.

At early stages (high T), the algorithm searches the parameter space in an essentially random manner. As T decreases, accepting increases in mismatch becomes less probable, and the algorithm spends more time searching regions of low mismatch, eventually converging to a solution which should approximate the global minimum.

The starting temperature, rate of reducing T, and the number and type of perturbations define the annealing schedule. Adopting an annealing schedule that is too fast (i.e., decreases T too quickly or allows too few perturbations) can lead to a sub-optimal solution. Alternatively, adopting a schedule that is too cautious wastes computation time. SA is a heuristic search technique, and there are a variety of

approaches to defining the annealing schedule. An appropriate annealing schedule is generally problem-specific and requires some experimentation and familiarity with the inverse problem.

Here, a variation of fast simulated annealing (Szu and Hartley 1987; ?), as implemented by Liu *et al.* (1995) is employed. Fast SA is based on using a temperature-dependent Cauchy distribution to generate the parameter perturbations, and geometrically reducing the temperature. The Cauchy distribution has the desirable properties of a Gaussian-like peak and Lorentzian tails which provides concentrated local sampling of the parameter space while allowing the occasional large perturbations. Each model parameter m_i is perturbed according to

$$m_i = m_i^{'} + \xi \Delta_i, \tag{3.3}$$

where $m_i^{'}$ is the value of the model parameter prior to the perturbation, Δ_i is a random variable uniformly distributed on the interval $[-\Delta m_i, \Delta m_i]$, where $\Delta m_i = m_i^+ - m_i^-$, and the quantity ξ is a Cauchy-distributed random variable as

$$\xi = [T_j/T_0]^{1/2} \tan[\pi(\eta - 1/2)]. \tag{3.4}$$

In Eq. 3.4, η is a uniform random variable on $[0, 1]$ and T_j is the temperature at the j^{th} step. The above procedure yields perturbations that are uniformly distributed in direction and Cauchy distributed in distance (in parameter space). The size of the perturbations decreases with the square root of the temperature (this is somewhat more conservative than the approach given by Szu and Hartley (1987) in which ξ depended directly on T). Thus, at high temperatures, large perturbations search the entire parameter space, while at low temperatures a more local search is performed. However, because of the long tails of the Cauchy distribution, large perturbations are possible at any temperature.

Each parameter is perturbed individually a pre-determined number of times according to Eq. 3.3 at each temperature step. The number of times each parameter is perturbed is chosen arbitrarily and generally requires some familiarity with the problem. After each perturbation, the change in mismatch is examined to determine if the new parameter is accepted or rejected. After a set of perturbations is complete, the temperature is reduced according to

$$T_j = \beta^j T_o, \tag{3.5}$$

where β is a positive constant less than one and T_o is the starting temperature. An appropriate value for T_o can be determined by requiring at least 90% of all perturbations (uphill and downhill) are accepted initially. Appropriate values for β and the number of perturbations per temperature step depend on the difficulty of the inversion and require some experimentation.

Once the desired number of iterations is completed, a process known as "quenching" is carried out to move to the bottom of the closest minimum. In quenching, the size of the model perturbations is held fixed and the temperature is set to zero for a preset number of iterations (this removes the possibility of taking uphill steps).

SA is an effective global optimization algorithm, but it does have a few shortcomings. It can be relatively inefficient near convergence and in cases where correlated parameters produce narrow valleys in the parameter space that are not aligned with the parameter axes. SA also lacks any form of memory, and therefore a good model may be discarded at an early stage and never revisited.

3.3 Simplex Simulated Annealing

Hybrid inversion algorithms combine local and global algorithms in an attempt to produce a more effective inversion technique. The goal of a hybrid algorithm is to

retain the advantages of each method while overcoming their respective weaknesses. SSA is a hybrid inversion which combines a local component based on the DHS method with a global SA optimization. A variety of hybrid algorithms have been developed for different types of geophysical inverse problems. For instance, Gerstoft (1995) used a combination of GA and the Gauss-Newton method for a geoacoustic inversion. Chunduru *et al.* (1997) used a conjugate gradient SA hybrid for a geo-electrical resistivity inversion problem. Liu *et al.* (1995) applied a weighted combination of DHS and SA to seismic waveform inversion. Finally, Press *et al.* (1992) suggested a somewhat different approach based on incorporating a random component directly into the local inversion at every step in a hybrid algorithm based on DHS and SA.

The SSA algorithm developed here incorporates the local DHS method described in Sec. 3.1 into the fast SA search described in Sec. 3.2. In particular, unlike standard SA, the SSA inversion operates on a simplex of models rather than a single model, and instead of employing purely random perturbations, DHS steps with a random component are applied to perturb the model. The procedure adopted here to introduce the random component into the DHS steps has proven to be very effective.

SSA begins with a randomly chosen simplex, referred to as the primary simplex. The DHS steps are not computed directly from the primary simplex, but rather from a secondary simplex which is formed by randomly perturbing all model parameters and mismatches of the primary simplex. To create the k^{th} model in the secondary simplex, the parameters of the k^{th} model in the primary simplex are perturbed according Eqs. 3.3 and 3.4. The mismatch associated with the k^{th} model of the secondary simplex is computed by perturbing the mismatch of the k^{th} model of the primary simplex according to

$$E = E' + \xi \bar{E}, \tag{3.6}$$

where E is the mismatch of the secondary simplex, E' is the mismatch of the primary simplex, $\bar{E}$ represents the mean mismatch of the primary simplex, and ξ is given by Eq. 3.4. For computational efficiency, the mismatches of the secondary simplex are computed by perturbing the primary values rather than by applying the forward model to the perturbed parameters. Using a secondary simplex of perturbed models and energies provided a more effective search of the parameter space.

The DHS steps proceed in a similar manner as in the standard DHS method. First, a reflection of the model with the highest mismatch is calculated and the new reflected model's mismatch is computed. This mismatch is compared to the highest mismatch of the primary simplex for acceptance using the probabilistic criterion of SA Eq. 3.2. This provides a mechanism for accepting uphill steps and escaping local minima. If necessary, the remaining steps (extension, contraction, multiple contraction) are performed. The accepted model(s) of the secondary simplex are used to replace the corresponding model(s) of the primary simplex. One additional constraint is applied: that the lowest-mismatch model of the primary simplex is never replaced by a higher-mismatch model. This provides the algorithm with a memory of the best model obtained to that point. A new secondary simplex is computed after each DHS step (accepted or rejected).

As in SA, the parameter search of the SSA algorithm is controlled by temperature. At high temperatures, the random component of the DHS steps dominates and the probability of accepting uphill steps is high, resulting in an essentially random search. At low temperatures, the random component and probability of accepting uphill steps is small, and the search approximates the local DHS method. At intermediate temperatures, the algorithm makes a smooth transition from a random search to the DHS method. Once the temperature has been reduced to a sufficiently low value, it is often effective to quench the inversion by setting the temperature to zero and using the DHS method to move directly to the bottom of the closest minimum. Figure 3.2 shows a block diagram illustrating the basic SSA algorithm.

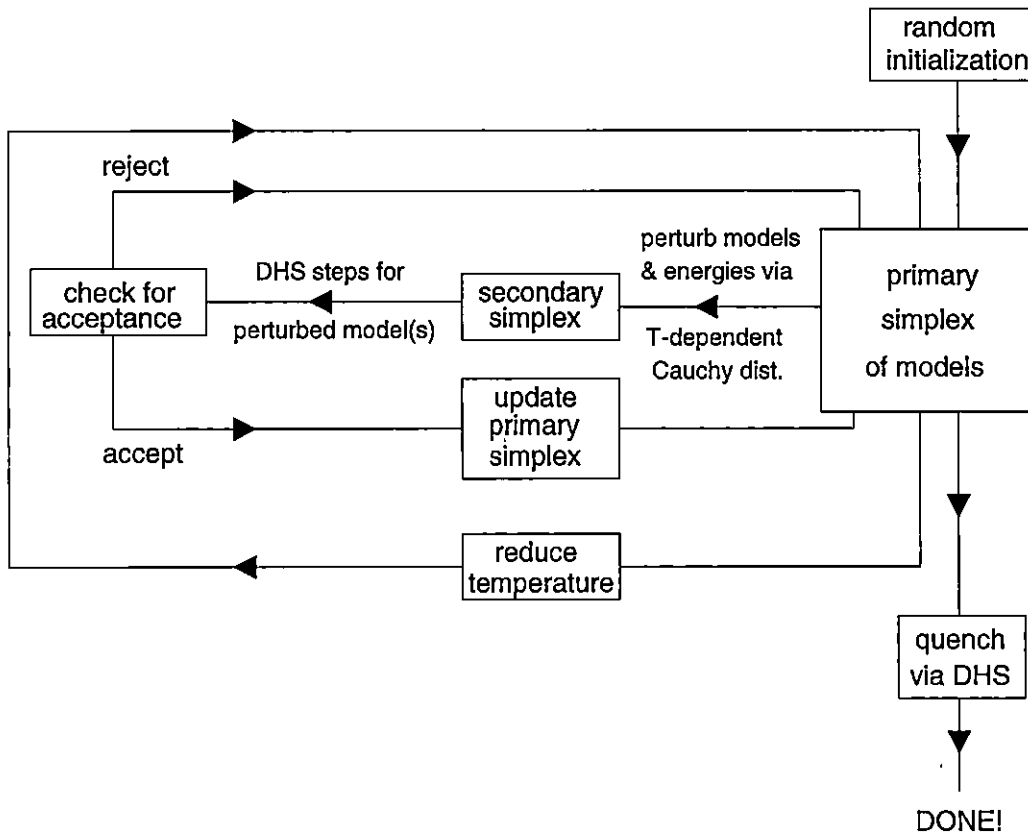

Figure 3.2 Simplified block diagram of the SSA algorithm.

A final comment about the SSA algorithm has to do with its efficiency. It should be noted that the most time-consuming step in the DHS method is the multiple contraction illustrated in Fig. 3.1 (e), since it requires the evaluation of the mismatch for all but one of the models in the simplex. In the early stages of the inversion, the additional computational expense of performing multiple contractions is generally wasted. Therefore, the efficiency of the SSA algorithm can be improved by introducing a simple procedure which allows only some fraction of multiple contractions to be performed. This fraction should be small (or zero) at high temperatures, and increased as temperature decreases, to a final value of unity near convergence.

SSA was developed to overcome the shortcomings associated with standard SA. Since DHS steps adjust all parameters at once according to the local gradient, the algorithm moves effectively down narrow oblique valleys in parameter space. Also, near convergence the algorithm more and more closely approximates the DHS algorithm and moves efficiently downhill. DHS and SA were chosen because each algorithm was simple and the resulting SSA algorithm was effective. In addition, since the current best model is always retained in the simplex, the algorithm has a form of memory. As a result of these features, the SSA algorithm can achieve substantially better results with a much faster annealing schedule than SA, as illustrated in the next chapter.

Chapter 4

Synthetic Data Inversion

In general, it is a good practice to validate a new inversion algorithm on synthetic data before applying it to experimental data. This way one can get a idea of how the algorithm is performing. It also offers a good arena in which to compare the algorithm to existing inversion techniques. Considering synthetic data can also give insight into a real-world problem (i.e., noisy measured data) by providing information such as parameter correlations and sensitivities, as well as helping to determine an effective annealing schedule.

In this chapter, the SSA algorithm is validated and compared with other inversion algorithms using a series of synthetic testcases. The first section describes the testcases the second section summarizes the results of the SSA inversions. The final section compares the SSA algorithm with DHS and SA. Appendix A presents a further comparison of the three algorithms using a multimodal function.

4.1 Synthetic Data

In June of 1997, a Matched-field Workshop (Workshop97, Tolstoy *et al.* 1998) was held to provide benchmark standards for the evaluation and comparison of various geoacoustic inversion algorithms. The synthetic data provided consisted of noise-free complex pressures on both vertical and horizontal sensor arrays. For each case, the data were divided into two frequency classes. The low-frequency data were given at 1 Hz intervals from 25 Hz to 199 Hz; the high frequency data were in 5 Hz intervals from 200 Hz to 500 Hz. The data were given at five ranges of 1–5 km for each class.

The data were computed using the numerical propagation model SAFARI (Schmidt 1988).

In this thesis, five different workshop testcases were studied. Three separate realizations existed for each testcase (denoted by the subscripts a, b, and c). The unknown parameter selection varied between the different testcases. For each realization, the value of the unknown parameters were randomly selected within the given search interval. The values were chosen randomly so that different inversion schemes could demonstrate their effectiveness for a range of parameter values (Tolstoy *et al.* 1998). This made some of the realizations more challenging because some parameters combinations led to difficulties (e.g., weak impedance contrast at the sediment/basement interface, Tolstoy *et al.* 1998; Fallat and Dosso 1998) and some parameter values were selected very close to the search boundary.

For four of the testcases (labeled SD, AT, SO and WA), the form of the geoacoustic model was exactly known (i.e., a single sediment layer over a semi-infinite basement). For these testcases the possible unknown parameters were chosen from: water depth, D; source range and depth, r and z; sediment thickness, h; compressional speed at the top and bottom of the sediment layer, c_0 and c_1 (linear gradient assumed); compressional speed of the basement, c_2; densities of the sediment and basement, ρ_1 and ρ_2; and attenuations of the sediment and basement, α_1 and α_2. Table 4.1 shows which unknown parameters were included in each testcase and Fig. 4.1 is a simple schematic of the ocean environment for these testcases. Table 4.2 shows the true parameter values for each realization while Table 4.3 gives the search intervals (m_i^- and m_i^+ are the upper and lower bounds for a given parameter).

The final testcase, labeled N, was a more challenging and practical testcase in that the form of geoacoustic model was not known and had to be included as part of the inversion. This testcase represented a general geoacoustic profile where an unknown number (N) of sediment layers overlaid a semi-infinite basement. In each sediment layer, the thickness, compressional speed, and density were unknown. In addition,

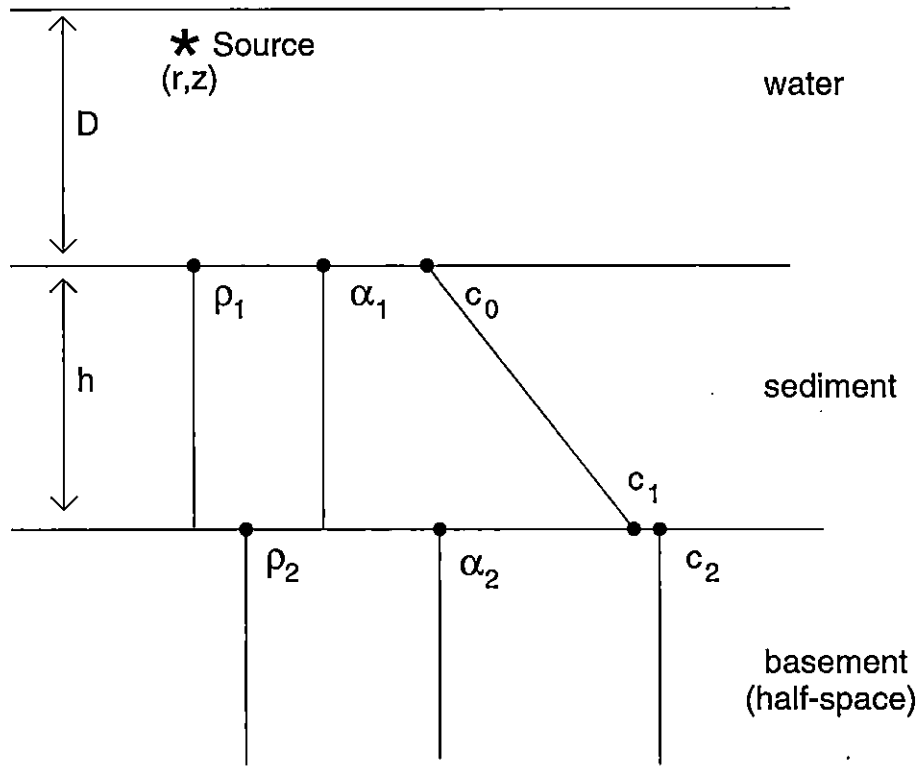

Figure 4.1 Schematic diagram of the ocean environment for the four testcases. The possible unknown parameters are indicated.

Table 4.1 The unknown parameters for workshop testcases SD, SO, AT and WA. The $\star$ indicates which unknown parameters were included in the geoacoustic model.

Case	h	c_0	c_1	c_2	ρ_1	ρ_2	α_1	α_2	D	r	z
SD	$\star$	$\star$	$\star$	$\star$	$\star$	$\star$					
AT	$\star$	$\star$	$\star$	$\star$	$\star$	$\star$	$\star$	$\star$			
SO	$\star$	$\star$	$\star$	$\star$	$\star$	$\star$				$\star$	$\star$
WA	$\star$	$\star$	$\star$	$\star$	$\star$	$\star$			$\star$	$\star$	$\star$

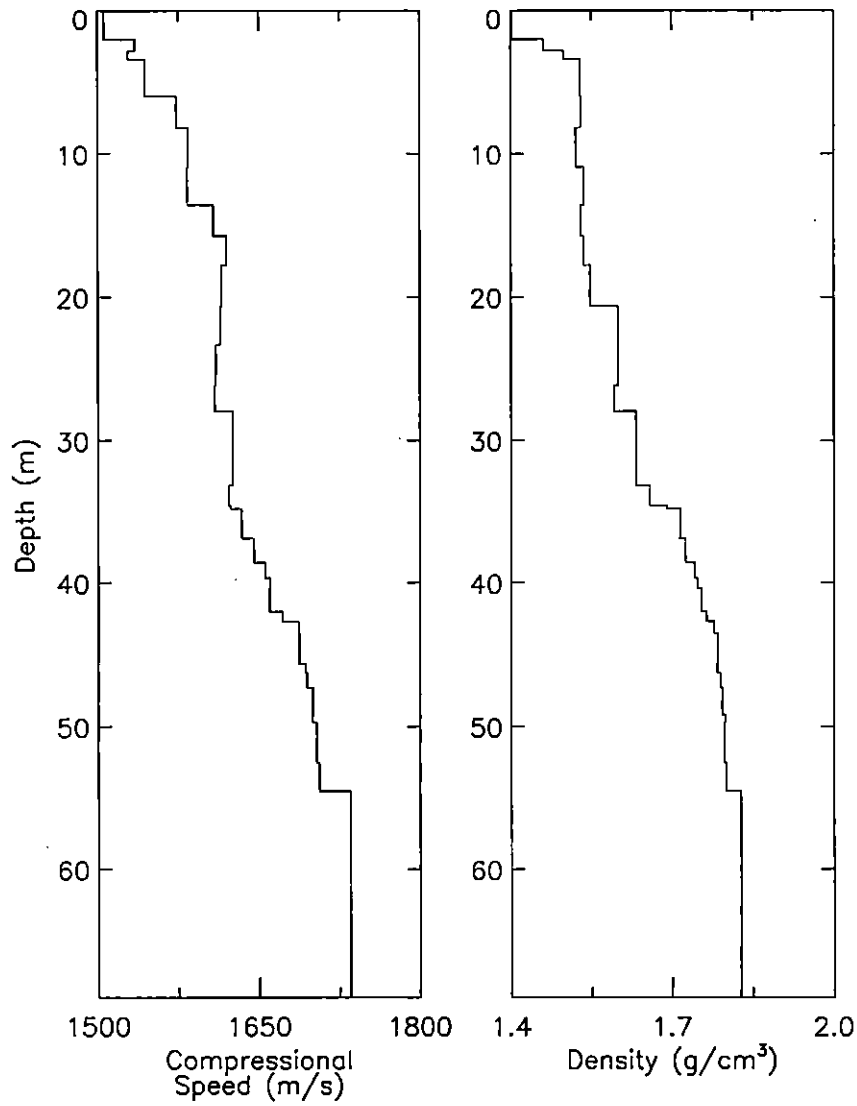

Figure 4.2 Workshop testcase N. All 34 sediment layers and portion a of the basement are shown.

the compressional speed and density of the basement were unknown. For this testcase there were 34 sediment layers over a semi-infinite basement (Fig. 4.2). The search limits for the N layer case are given in Table 4.4.

Table 4.2 The true parameter values for each realization for the four workshop testcases.

Case	h (m)	c_0 (m/s)	c_1 (m/s)	c_2 (m/s)	ρ_1 (g/cm^3)	ρ_2 (g/cm^3)			
SD_a	22.4678	1565.12	1743.14	1757.69	1.75528	1.83349			
SD_b	38.0407	1599.33	1658.46	1707.46	1.64407	1.86593			
SD_c	30.6873	1530.44	1604.15	1689.00	1.50088	1.70064			
	h (m)	c_0 (m/s)	c_1 (m/s)	c_2 (m/s)	ρ_1 (g/cm^3)	ρ_2 (g/cm^3)	α_1 (dB/λ)	α_2 (dB/λ)	
AT_a	44.5700	1546.91	1624.75	1676.30	1.40277	1.77546	0.123680	0.080461	
AT_b	13.4381	1558.27	1564.62	1758.80	1.77156	1.95231	0.314234	0.198221	
AT_c	30.3733	1533.93	1557.58	1615.15	1.42907	1.68715	0.083998	0.052783	
	h (m)	c_0 (m/s)	c_1 (m/s)	c_2 (m/s)	ρ_1 (g/cm^3)	ρ_2 (g/cm^3)	r (km)	z (m)	
SO_a	22.2709	1592.64	1698.67	1743.96	1.60528	1.80280	1.38	25.0818	
SO_b	35.9918	1510.36	1745.47	1768.94	1.47128	1.91394	1.18	15.3150	
SO_c	46.8737	1541.75	1674.23	1764.42	1.49732	1.87081	1.04	27.9474	
	h (m)	c_0 (m/s)	c_1 (m/s)	c_2 (m/s)	ρ_1 (g/cm^3)	ρ_2 (g/cm^3)	r (km)	z (m)	D (m)
WA_a	27.079	1516.20	1573.15	1751.26	1.5379	1.8518	1.220	26.420	115.334
WA_b	31.841	1584.32	1722.68	1778.95	1.8033	1.8643	1.105	26.515	106.721
WA_c	28.953	1565.69	1591.76	1707.12	1.6789	1.8844	1.290	28.230	119.879

Table 4.3 The search bounds for the workshop testcases, where m_i^- represents the lower bound and m_i^+ represents the upper bound.

Parameter	m_i^-	m_i^+	Parameter	m_i^-	m_i^+
h	10	50	α_1	0.05	0.5
c_0	1500	1600	α_2	0.05	0.5
c_1	1550	1750	r	1.0	1.4
c_2	1600	1800	z	10	30
ρ_1	1.4	1.85	D	100	120
ρ_2	1.6	2.0			

Table 4.4 The search bounds for the workshop testcase N, where m_i^- represents the lower bound and m_i^+ represents the upper bound.

Bound	h_i	c_i	ρ_i	c_b	ρ_b	N
	(m)	(m/s)	(g/cm^3)	(m/s)	(g/cm^3)	
m_i^-	0.0	1500	1.4	1600	1.6	1
m_i^+	3.0	1600	2.0	1800	2.0	50

4.2 Validating Simplex Simulated Annealing

In this section, the results of the SSA inversions for the Workshop97 testcases are presented. Since the testcases were synthetic (no noise) and the true parameter values were exactly known, it was an extremely useful set of data to validate the SSA algorithm. SSA was applied to four testcases where the form of the geoacoustic was known (SD, AT, SO, and WA), and to testcase N which represented a general geoacoustic profile.

The replica fields for the inversions were computed using the forward model ORCA (Westwood *et al.* 1996). For these testcases, the Bartlett mismatch (Eq. 2.4) between SAFARI- and ORCA-generated fields when the true parameter values were used was $E \sim 1.0 \times 10^{-6}$. This model-based mismatch places a lower limit on the useful range of inversion mismatch values (i.e., it is not meaningful to invert data to $E < 1.0 \times 10^{-6}$).

Case SD was the simplest testcase with only six unknown parameters. The data used in the inversion consisted of acoustic pressure fields at a frequency of 100 Hz measured at a VLA of 20 hydrophones evenly spaced in the water column. The water depth was 100 m, the source depth was 20 m and the source range was taken to be 1 km. The VLA configuration, water depth and source position described here are the same for the other testcases, unless one of these parameters are considered unknown. Excellent results were obtained for all three realizations of testcase SD. The results were characterized by exceedingly low levels of mismatch and estimates

Table 4.5 The inversion results for each realization for each of the four workshop testcases. The final column (E) is the mismatch obtained in the inversion. This result represents the model in the simplex which achieved the lowest mismatch.

Case	h (m)	c_0 (m/s)	c_1 (m/s)	c_2 (m/s)	ρ_1 (g/cm^3)	ρ_2 (g/cm^3)	E			
SD_a	21.9	1565	1737	1758	1.76	1.81	2.9e−6			
SD_b	38.1	1599	1659	1706	1.65	1.88	2.3e−6			
SD_c	30.7	1530	1604	1689	1.50	1.70	1.1e−6			
	h (m)	c_0 (m/s)	c_1 (m/s)	c_2 (m/s)	ρ_1 (g/cm^3)	ρ_2 (g/cm^3)	α_1 (dB/λ)	α_2 (dB/λ)	E	
AT_a	44.7	1547	1626	1676	1.40	1.78	0.13	0.11	2.9e−6	
AT_b	13.4	1559	1563	1759	1.77	1.94	0.31	0.20	1.4e−6	
AT_c	30.4	1535	1557	1615	1.43	1.68	0.08	0.11	3.7e−6	
	h (m)	c_0 (m/s)	c_1 (m/s)	c_2 (m/s)	ρ_1 (g/cm^3)	ρ_2 (g/cm^3)	r (km)	z (m)	E	
SO_a	21.9	1594	1692	1745	1.61	1.68	1.38	25.1	1.1e−6	
SO_b	35.6	1511	1740	1772	1.46	1.69	1.18	15.3	2.9e−5	
SO_c	46.9	1541	1675	1757	1.51	1.89	1.04	28.0	1.8e−5	
	h (m)	c_0 (m/s)	c_1 (m/s)	c_2 (m/s)	ρ_1 (g/cm^3)	ρ_2 (g/cm^3)	r (km)	z (m)	D (m)	E
WA_a	27.1	1517	1573	1751	1.54	1.81	1.22	26.4	115.4	3.0e−6
WA_b	33.1	1582	1734	1775	1.82	1.85	1.10	26.5	106.7	1.6e−5
WA_c	28.8	1568	1589	1708	1.66	1.77	1.29	28.2	119.9	3.2e−5

of the parameter values that were close to the true values. This included realization SD_a which proved to be quite difficult to invert using other techniques (Tolstoy *et al.* 1998; Fallat and Dosso 1998). The inversion results are summarized in Table 4.5 and Fig. 4.3 shows the results for case SD_a. For this figure all models and energies in the simplex are plotted as they progress through the inversion. The dotted lines indicate the true parameter values and the range of ordinate values represent the given search intervals.

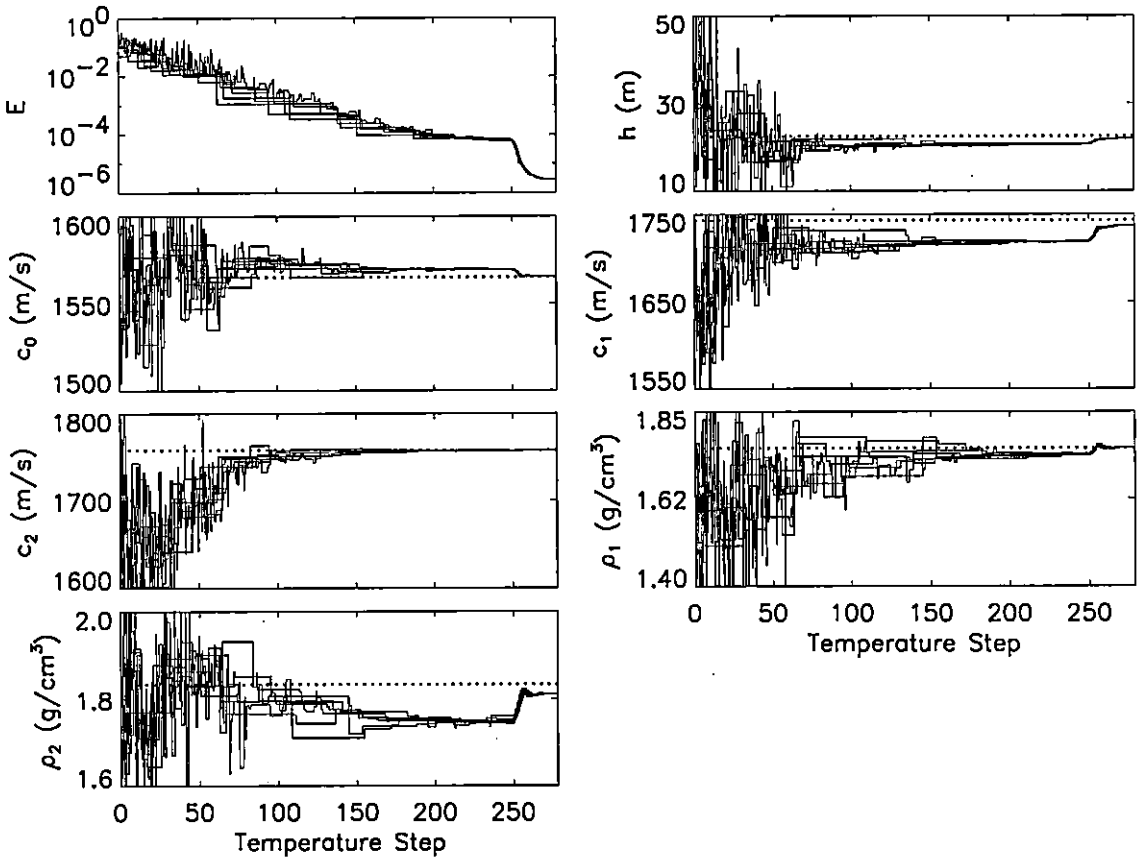

Figure 4.3 Convergence of mismatch E and model parameters for case SD_a. The dotted line indicates the true parameter value, and the range of ordinate values indicates the parameter search interval.

The AT testcase was somewhat more difficult because it included the attenuations in the sediment and basement as unknown parameters. Therefore, there were eight parameters in the geoacoustic model. For each realization, SSA produced good estimates for all model parameters except the basement attenuation for case AT_c. Figure 4.4 shows the inversion results for case AT_a and the results of all three realizations are summarized in Table 4.5.

SO had eight model parameters, but instead of attenuations, the source range and depth were taken as unknowns. For realization SO_a, the inversion results are quite good. For SO_b and SO_c the inversions obtained a higher level mismatch then SO_a and the estimates of the model parameter are not as good. For sensitive parameters, such as source range and depth and sediment thickness, the estimates are very good, but for insensitive parameters, like basement density, the estimate is relatively poor. The results for testcase SO are still good, even though the mismatches are slightly higher. The results of the inversion for SO_a are shown in Fig. 4.5 and Table 4.5 summarizes the results of SO_a, SO_b and SO_c.

Testcase WA case had nine unknown parameters which included the same eight as case SO as well as the water depth. WA proved to be the most challenging of the testcases because it had nine unknown parameters with a large range of sensitives. Figures 4.6 and 4.7 show one dimensional (1-D) and 2-D cross sections of the parameter space for the WA_a case. For each figure, the parameters that are not varied are held fixed at their true value. These figures clearly illustrate that there are a large number of local minima, correlations between parameters (resulting in narrow oblique valleys not aligned with the parameter axes), and a wide range of parameter sensitives.

The inversion results for case WA are good. Realization WA_a has a very low mismatch and the estimates for the true parameter values are very well determined. For WA_b and WA_c the results are still quite good with the exception of the basement density for WA_c. Figure 4.8 shows the result of the SSA inversion for case WA_a while

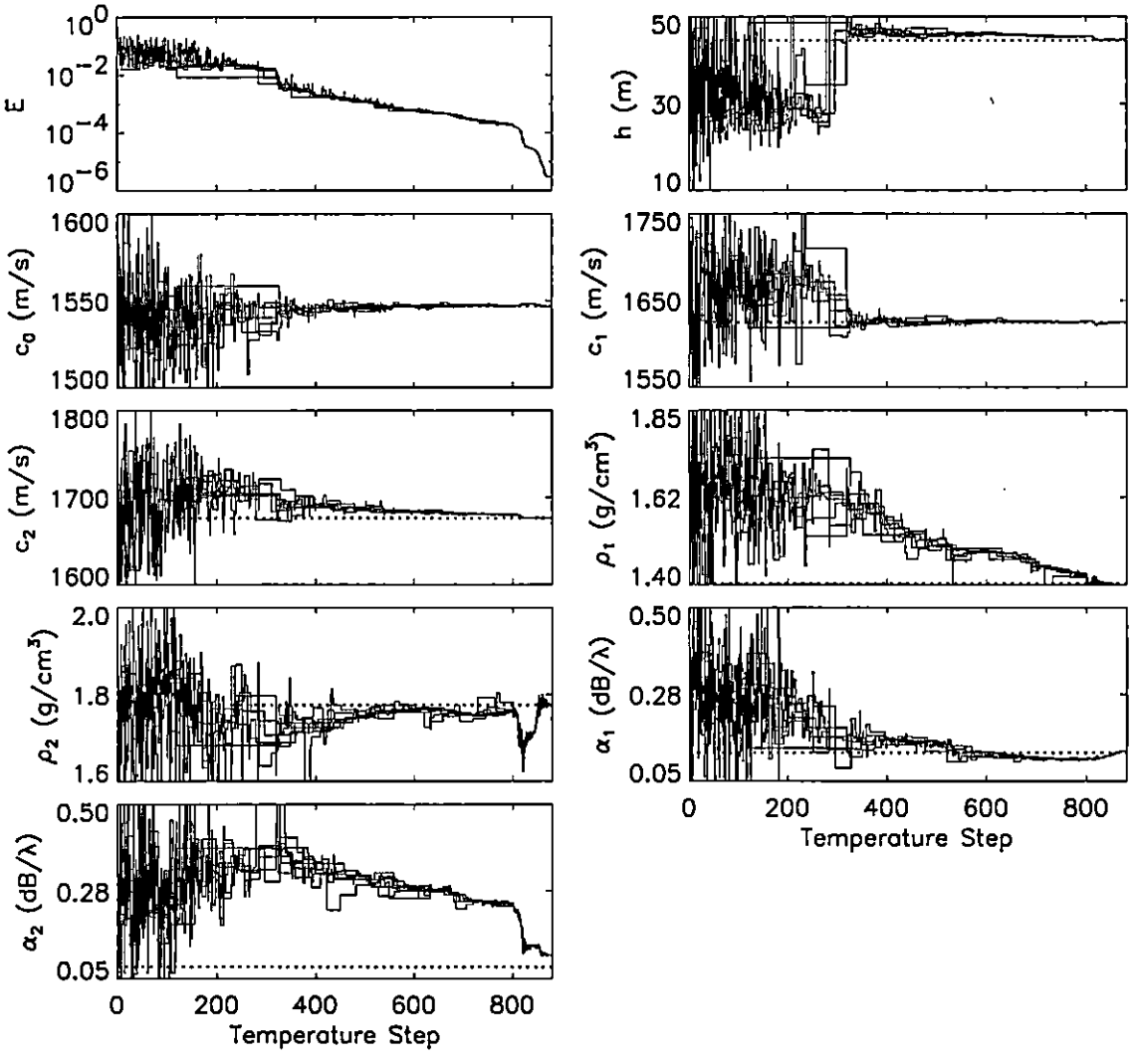

Figure 4.4 Convergence of mismatch E and model parameters for case AT_a.

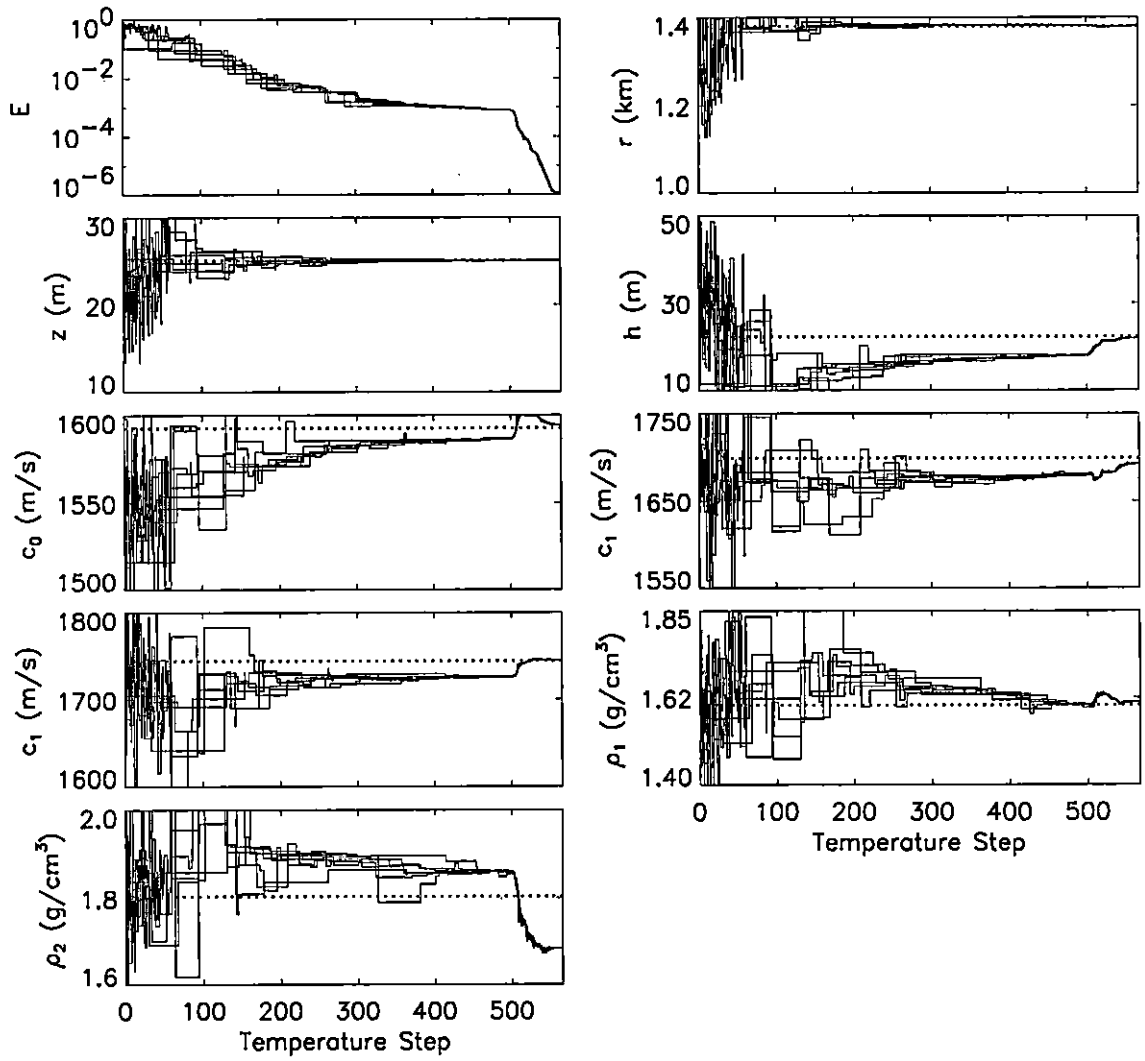

Figure 4.5 Convergence of mismatch E and model parameters for case SO_a.

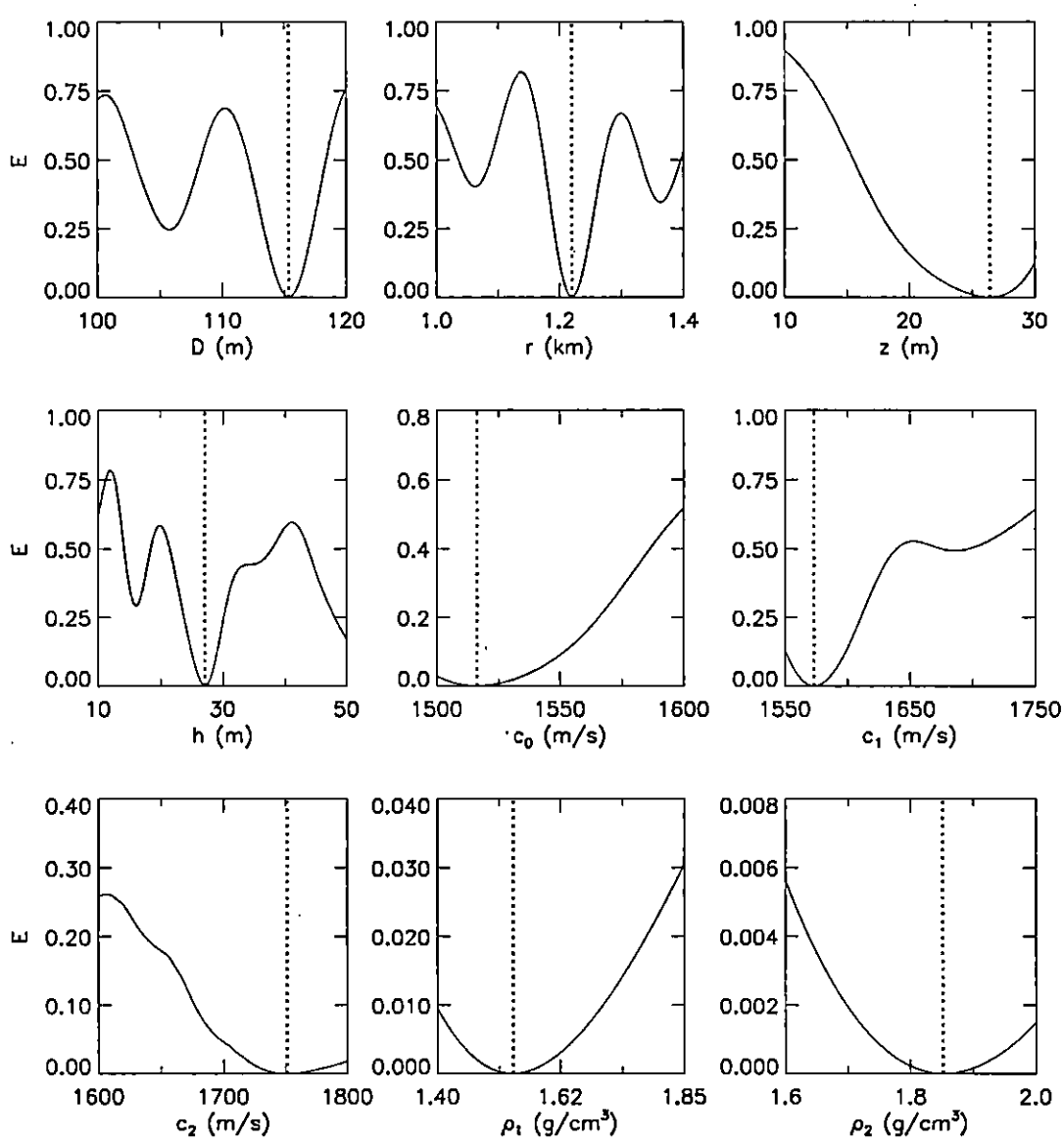

Figure 4.6 1-D cross sections of the parameter space for the WA_a case. The dotted line represents the true parameter value. The range of parameter sensitivities is clearly seen by comparing D and ρ_1.

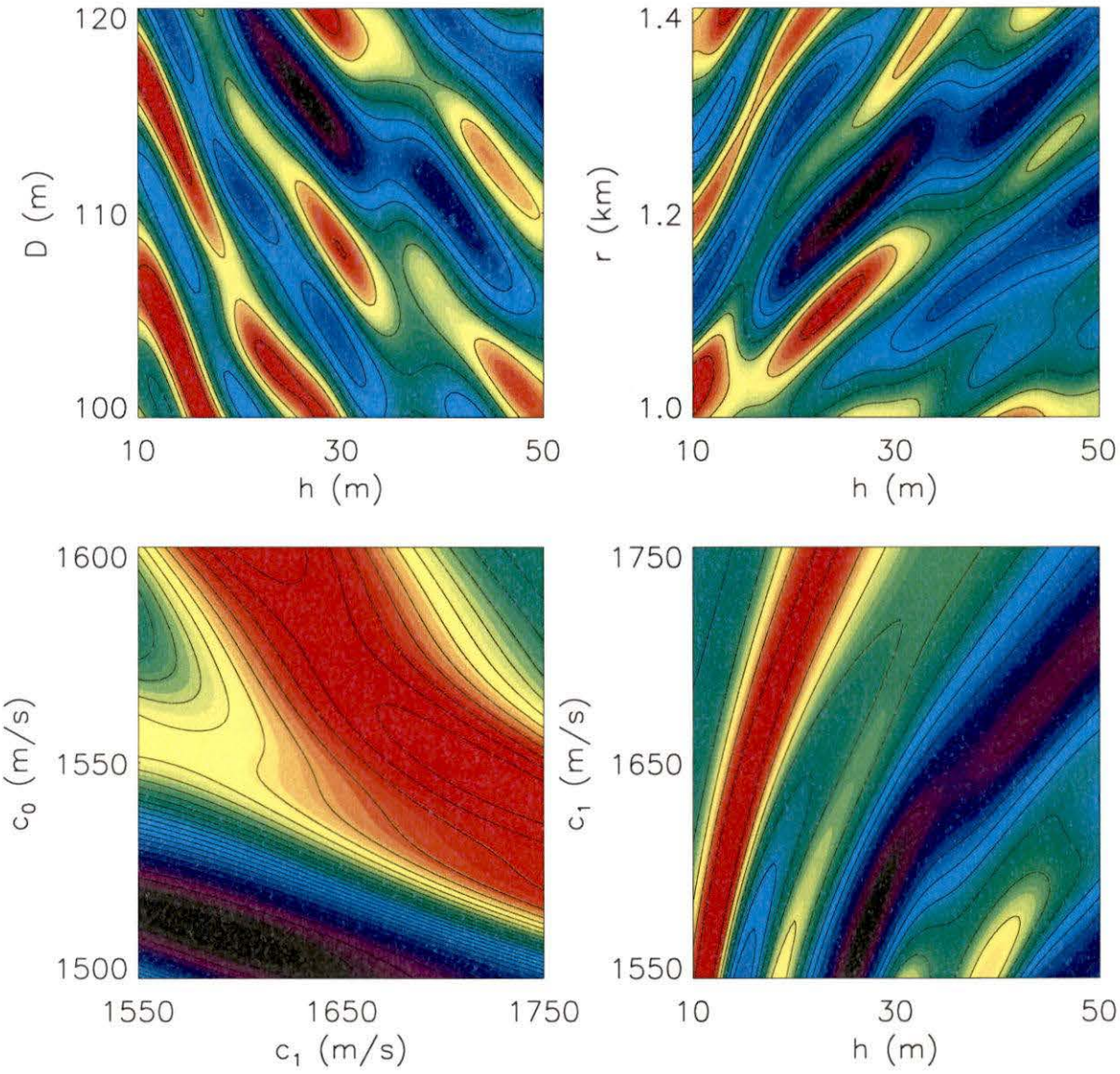

Figure 4.7 2-D cross sections of the parameter space for the WA_a case selected to illustrate local minima and correlations between parameters. The black and blue regions represent low mismatch while the yellow and red represent high mismatch.

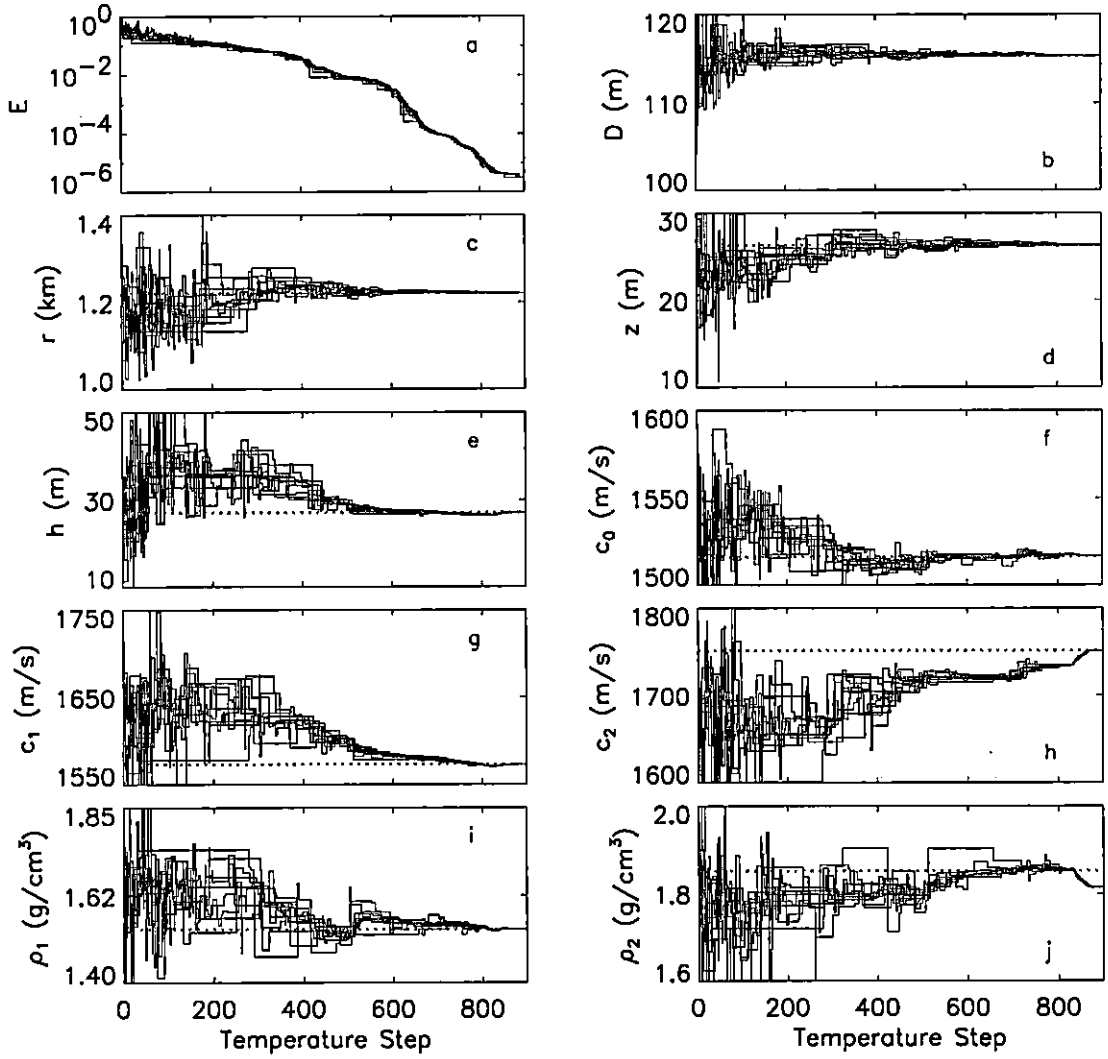

Figure 4.8 Convergence of mismatch E and model parameters for case WA_a.

the results of all three realizations are given in Table 4.5.

4.2.1 N Layer case: General geoacoustic profile

The final workshop testcase that SSA was applied to was testcase N. This case had an unknown (large) number of sediment layers, representing a general geoacoustic profile. When the model structure is not known it is well-advised to seek as simple a solution as possible (i.e., minimum-structure solution). There are two general approaches to accomplish this. One is to control the amount of structure by the parameterization of the model. A typical application of this approach begins by inverting an under-parameterized model, and then successively repeats the inversion as the number of model parameters is increased until a point is reached where further increases in parameters leads to negligible decreases in mismatch. Beyond this point, including more parameters allows more structure; however, this structure is clearly not required by the data. The other approach is to over-parameterize the model, but to include an explicit penalty for model structure along with data mismatch in the objective function being minimized (i.e., regularize the inversion by minimizing model structure). A well-developed theory for this approach exists for local inverse methods (Constable *et al.* 1987); however, applications to global inversion to date are somewhat ad hoc (Dosso *et al.* 1993a).

In this thesis, an under-parameterized approach is applied. The VLA configuration, water depth and source position are the same as the previous testcases, but for this case data at two frequencies of 40 and 120 Hz were used. The problem consisted of inverting the data for compressional-speed and density profiles (including the basement); the source position and water depth were considered known. The parameters included in the inversion were the compressional speed, density, and the thickness of each sediment layer and the compressional speed and density of the basement. Hence, for a model of N layers, there are a total of $3N - 1$ unknown parameters. For this case the model which produces the best trade-off between a low mismatch and a small amount of structure will be the best parameterization.

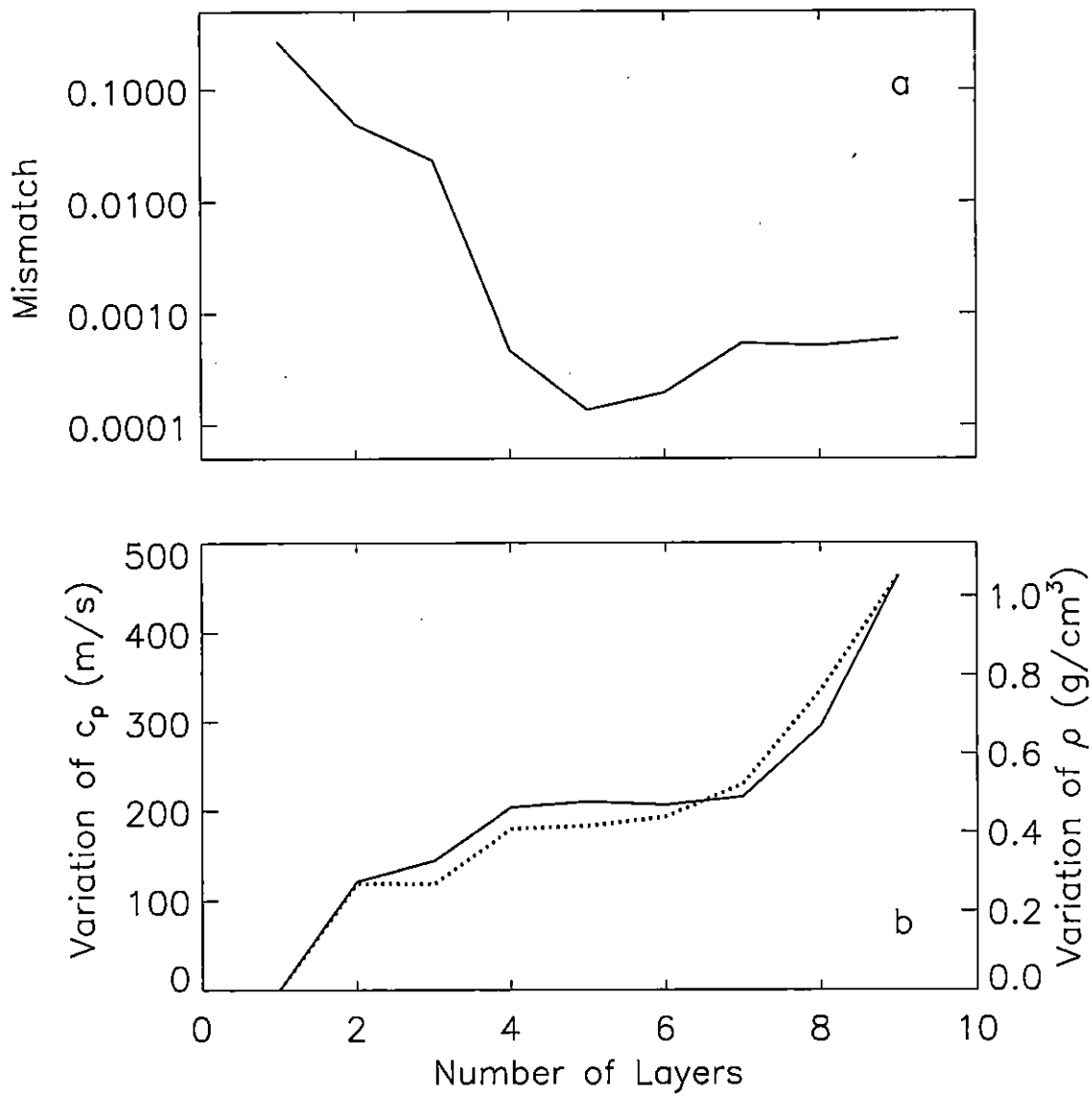

Figure 4.9 The mismatch for case N as a function of the number of layers included in the inversion is shown in (a). The L_1 norm of the variation of the compressional speed c_p and density ρ is indicated by the solid and dotted lines, respectively, in (b).

Figure 4.9 (a) shows the mismatch obtained in the inversions when the model consisted of 1–9 layers (including the basement). The mismatch in Fig. 4.9 (a) decreases significantly as the number of layers increases from one to five; beyond five layers the mismatch increases slightly. This slight increase is likely due to the fact that as the number of model layers increases beyond the number that are well resolved by the data, the number of local minima in the parameter space increases greatly, and the SSA inversion algorithm has increasing difficulty finding a good approximation to the global minimum. Adding more layers allows the amount of model structure to increase. The structure of the geoacoustic profile can be quantified by the L_1 norm of the variation:

$$V = \sum_{i=1}^{N-1} |q_{i+1} - q_i|, \tag{4.1}$$

where q represents either the compressional speed or density and N is the number of layers. Figure 4.9 (b) shows the variation of the compressional speed (solid) and density (dotted) as a function of the number of layers included in the model. The variation increases as the number of layers is increased from one to four. For four to seven layers, the variation remains approximately constant; for more than seven layers the variation again increases with the number of layers. This increase in variation is illustrated in Fig. 4.10 which shows examples of the compressional-speed and density profiles obtained by the SSA inversion for two, five, and nine layers. In each case the dotted line indicates the inversion result and the solid line indicates the true profile.

The two-layer model Fig. 4.10 (a) and (b) represents a reasonable, if somewhat simplified, approximation to the true profiles. A good approximation of the true profiles is obtained for the inversion that included five layers in the model Fig. 4.10 (c) and (d). The nine-layer case produced a reasonable estimate of the compressional-speed profile Fig. 4.10 (e), but produced a relatively poor estimate of the density profile Fig. 4.10 (f). Also, the nine-layer case clearly contains extra structure, in the

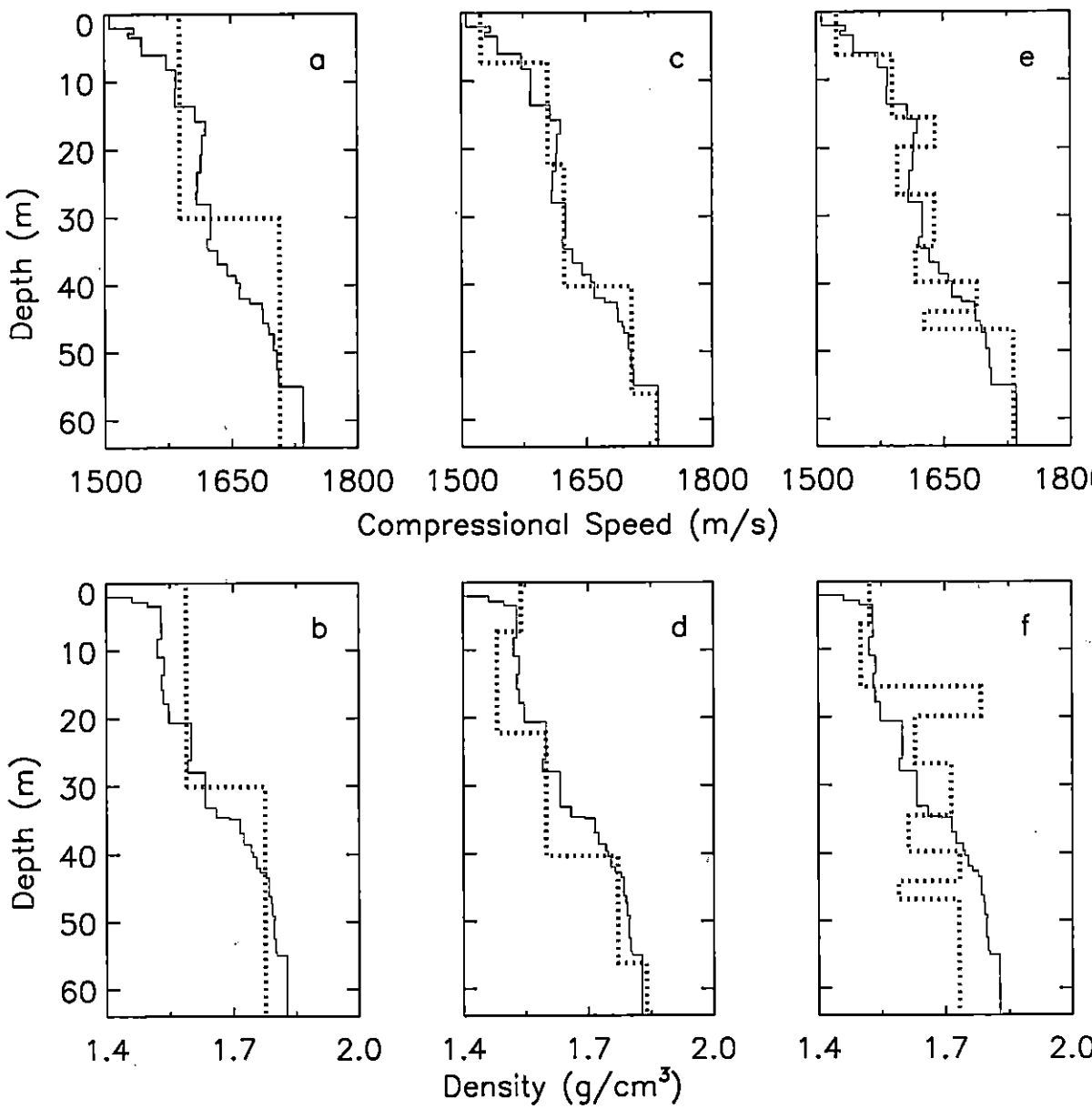

Figure 4.10 Compressional speed and density profiles obtained by SSA inversion. The inversion results for two, five, and nine layers are shown by the dotted lines in (a, b), (c, d) and (e, f) respectively. The solid lines are the true compressional speed and density profiles

form of thin low-speed and/or high- and low-density layers.

According to Figs. 4.9 and 4.10, the five-layer model would seem to achieve the best trade-off between a low mismatch and a small amount of structure, and hence is the preferred interpretation. To investigate the range of possible five-layer solutions, the SSA inversion was repeated ten times from different starting points. Figure 4.11 shows the results of these inversions. The inversions produced consistently good estimates for the compressional speed profile Fig. 4.11 (a), with a tight envelope closely following the true profile. Since the data are relatively insensitive to the sediment density, the density profile is not as well constrained (Fig. 4.11 b); however, the underlying trend of the density increasing with depth is clearly evident.

4.3 Comparison with Simulated Annealing and Downhill Simplex Method

In this section, the SSA algorithm is compared with the DHS method and SA. The testcase WA_a was used for the comparison. Section 4.2 showed that this testcase involved three important features that make the inversion difficult: a large number of local minima, correlations between some parameters, and a wide range of parameter sensitivities (see Figs 4.6 and 4.7). A further comparison of the algorithms is contained in Appendix A.

Since DHS is a local method, it moves continuously downhill but as it does not have a mechanism to move uphill, it is prone to getting trapped in local minima. Therefore, to properly apply the DHS method to geoacoustic inversion it is necessary to initiate the algorithm from a number of starting models. Using this strategy, the model solution that attains the lowest mismatch is taken as the best estimate of the true parameter values.

Figure 4.12 shows the compilation of the final model parameters obtained by initiating the DHS algorithm from 250 randomly chosen starting simplexes (i.e., 2500

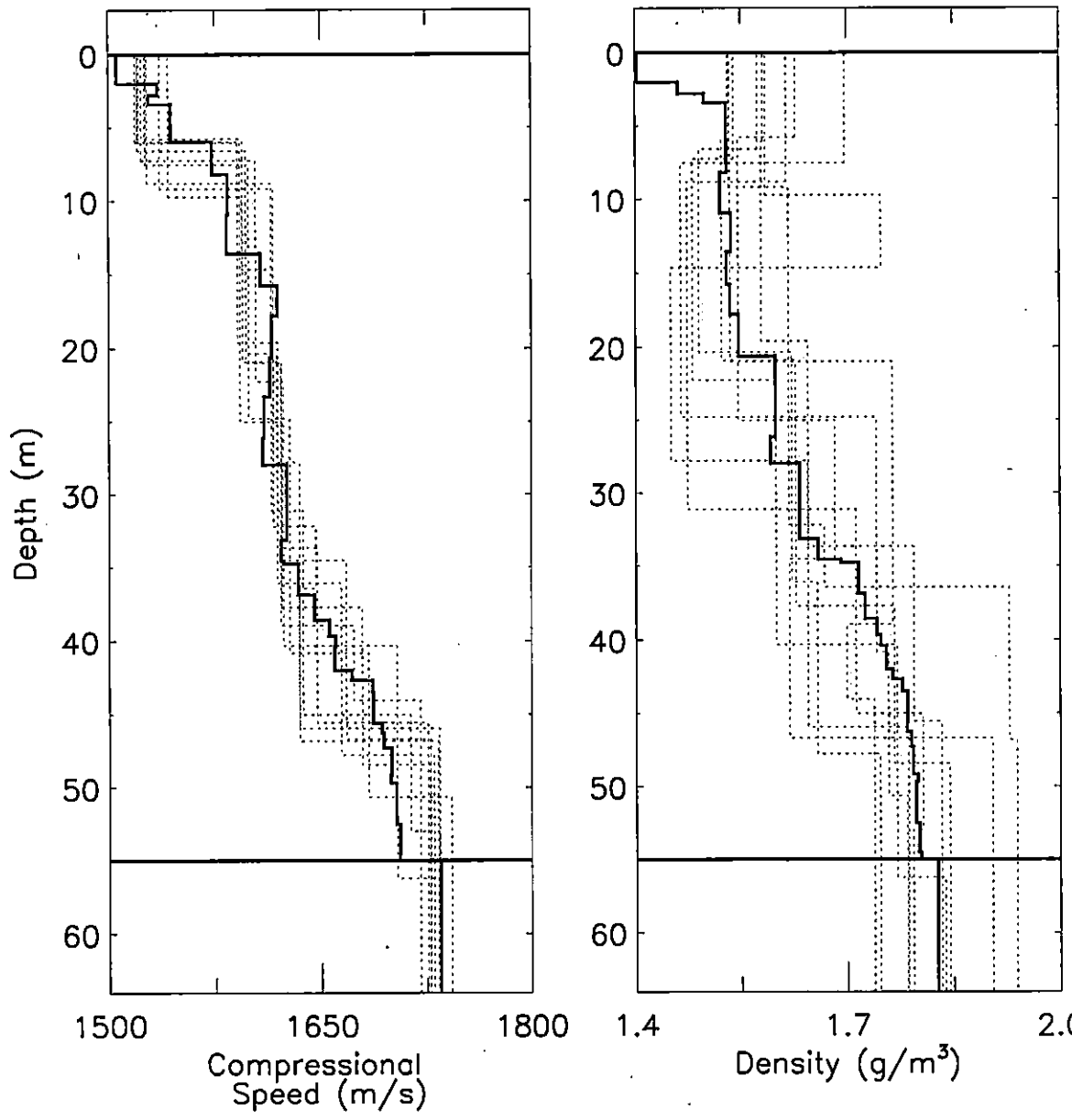

Figure 4.11 Results of ten SSA inversions showing (a) compressional speed and (b) density profiles. The dotted lines are the inversion result, the solid line indicates the true profile.

Table 4.6 The true parameter values and the inversion results for DHS, SA, and SSA for the case WA_a. CPU indicates the computation time for the inversion.

Case	h (m)	c_0 (m/s)	c_1 (m/s)	c_2 (m/s)	ρ_1 (g/cm^3)	ρ_2 (g/cm^3)	D (m)	r (km)	z (m)	E	CPU (hrs)
True	27.1	1516	1573	1751	1.54	1.85	115.3	1.22	26.4	–	–
DHS	27.1	1516	1574	1751	1.54	1.88	115.3	1.22	26.4	2.6e−6	30
SA	27.5	1518	1572	1761	1.52	1.71	115.4	1.22	26.4	1.4e−4	12
SSA	27.1	1517	1573	1751	1.54	1.81	115.4	1.22	26.4	3.0e−6	1

random starting models, since there are 10 models in each simplex). The tolerance used for convergence according to Eq. 3.1 was $\varepsilon = 10^{-3}$ and a maximum of 1000 iterations were allowed which lead to all but three of the cases running to convergence. The inversion required $\approx$ 30 hours of computation time on a 200 MHz Pentium PC.

The plots in Fig. 4.12 show the mismatch as a function of model parameter. The range of abscissa values indicates the parameter search interval and the true parameter values are given by the dotted line. The algorithm frequently obtained models with relatively low mismatch, with 40% of the solutions achieving mismatches of $E < 10^{-2}$ and 20% obtaining $E < 10^{-3}$. The sensitive parameters D, h, r and z are generally well determined, with reasonable estimates obtained for $E \lesssim 10^{-2}$. The compressional speeds c_0, c_1 and c_2 are fairly well determined for $E \lesssim 10^{-3}$. However, the densities ρ_1 and ρ_2 are generally poorly determined: even with $E < 10^{-4}$ good estimates for ρ_2 are not always obtained. The set of model parameters which achieved the smallest mismatch ($E = 2.6 \times 10^{-6}$) is given in Table 4.6 and represents excellent estimates for all parameters. Note the mismatch approaches the level of model-based mismatch.

SA was the next algorithm applied to the WA_a data. The annealing schedule (see Sec. 3.2) was initiated at a temperature of $T_o = 0.3$ and involved 2500 iterations (temperature steps) with five perturbations of each parameter at each iteration, and a temperature reduction factor of $\beta = 0.995$. The inversion required $\approx$ 12 hours of

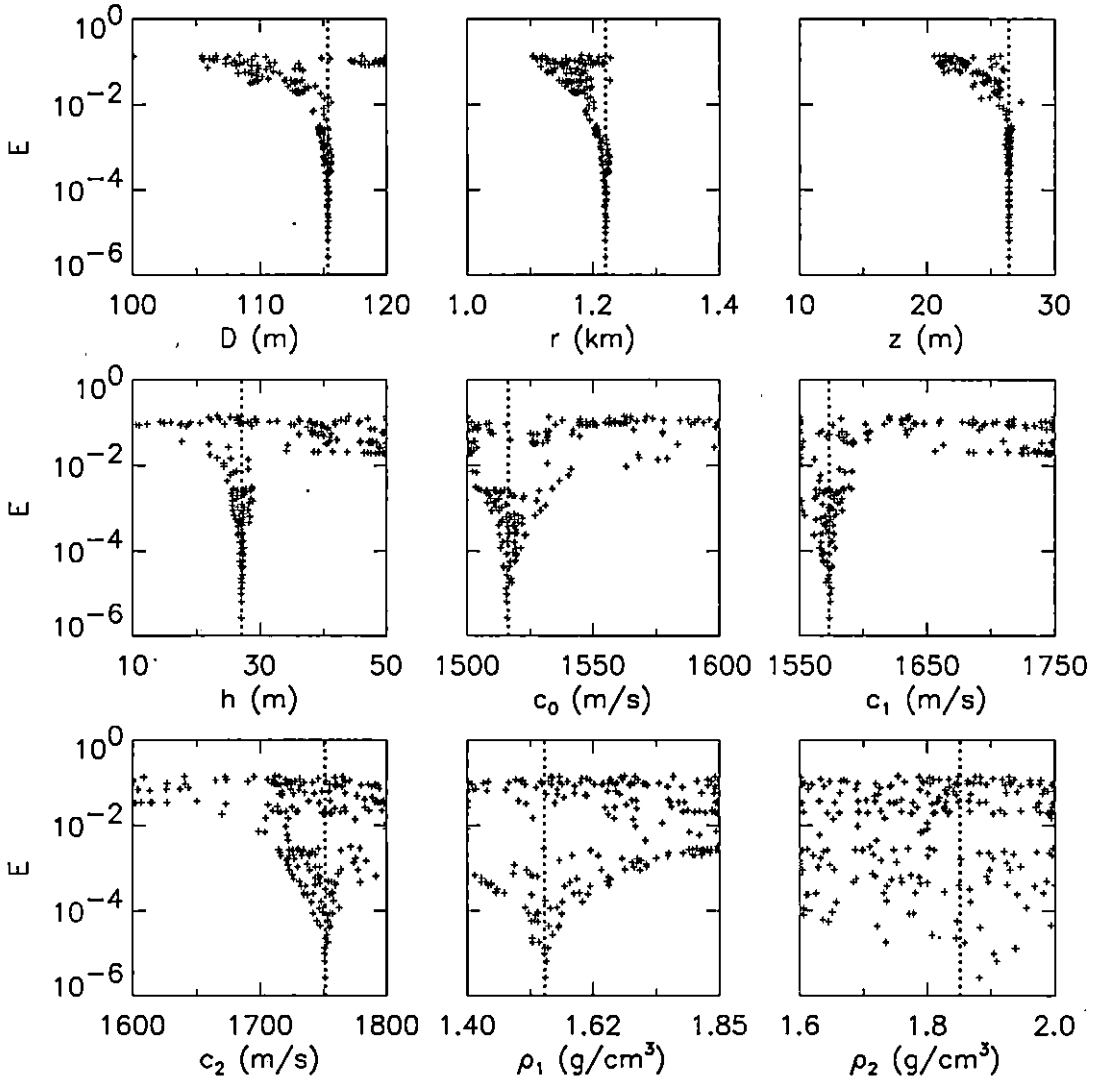

Figure 4.12 Results for 250 independent DHS inversions for WA_a. The dotted line represents the true parameter values, and the range of abscissa values indicates the parameter search interval.

computation time. The results of the inversion are shown in Fig. 4.13 and summarized in Table 4.6. Figure 4.13 (a) shows that the mismatch E decreases steadily (although not monotonically) with temperature to a small final value of 1.4×10^{-4}. Figure 4.13 (b)–(j) shows the convergence of the geoacoustic parameters. Good estimates of the true values are found for all parameters, with the exception of the basement density ρ_2.

SSA was applied to testcase WA_a in Sec. 4.2, the results are summarized in Fig. 4.8 and Table 4.5. For this inversion, the annealing schedule was initiated at a temperature of $T_o = 0.3$ and involved 800 iterations (temperature steps) with three DHS steps at each iteration and a temperature reduction factor of $\beta = 0.985$. A rule of thumb can be used to determine an estimate of the number of forward model evaluations used in the inversion, take the number of iterations multiplied by the number of DHS steps at each iteration and multiply this by 2 or 3. The inversion required 1 hour of computation time. The final mismatch for the inversion is very low (3.0×10^{-6}) and approaches the level of model-based mismatch. The SSA inversion produced excellent estimates of the true values for all the unknown parameters, including the basement density.

Overall, SSA proved to be very effective for inverting the Workshop97 testcases. For the first four testcases where the form of the geoacoustic model was known (SD, AT, SO, and WA) the inversion produced excellent estimates of the true model parameters. The only exceptions were insensitive parameters such as basement density and the attenuations. For the more practical testcase (N) which consisted of inverting for an unknown number of sediment layers, SSA produced reasonable estimates for the true model parameters. An under-parameterized approach was employed for this inversion to determine the model which achieved the best trade-off between low mismatch and simple structure. Therefore, the model SSA produced had fewer layers then the true model, but was still a good approximation to the true model.

SSA was also compared with DHS and SA using one of the workshop testcases.

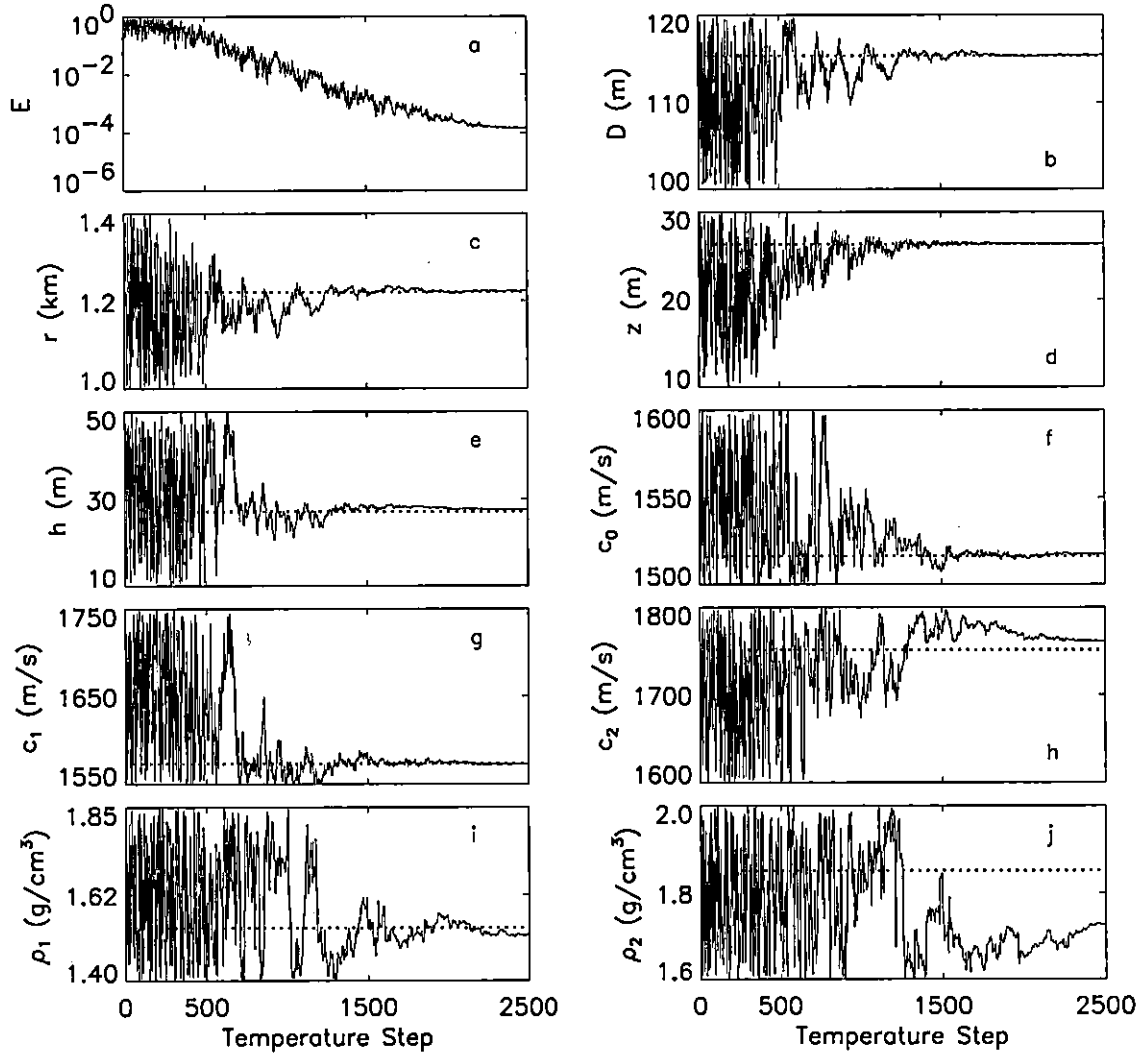

Figure 4.13 Convergence of the mismatch E and model parameters for the SA inversion. The dotted line represents the true parameter value, and the range of ordinate values indicates the parameter search interval.

In both cases SSA produced as good or better results as DHS and SA in at least an order of magnitude less computation time. This decrease in computation time was accomplished by SSA requiring far fewer forward model evaluations. Fallat and Dosso (1998) applied a fast SA algorithm to all the workshop testcases (except the N layer case) with good results. Without exception SSA produced better results than the fast SA algorithm with fewer forward model evaluations.

Chapter 5

Experimental Data Inversion

In 1997, SACLANT Undersea Research Centre conducted a geoacoustic experiment, PROSIM'97, off the west coast of Italy. The experiment was conducted in a region where a good deal of ground truth information existed (Akal *et al.* 1970; Akal *et al.* 1972) and where previous inversion experiments had been performed (Hermand and Gerstoft 1996; Siderius and Hermand 1999). The goal of this chapter was to apply the SSA algorithm to some of the acoustic data to determine estimates of the geoacoustic and geometric properties of the experiment.

This chapter describes the inversion of a portion of the acoustic data recorded during this experiment. First, a general description of the experiment is given, followed by a discussion of the synthetic data inversions that were run. The third section contains the description of the experimental data inversion including a discussion of the results. The final section compares these inversion results with the results of previous experiments from the same area.

5.1 Experiment Description

The PROSIM'97 experiment (Nielsen *et al.* 1998) was part of the European Community funded MAST III project. It was conducted between 15–23 of May 1997, in the region south-east of Elba Island in the Mediterranean Sea off the western coast of Italy (Fig. 5.1). Environmental data such as water temperature, sound speed, current velocity, sea surface wave height, and weather conditions were recorded throughout the experiment.

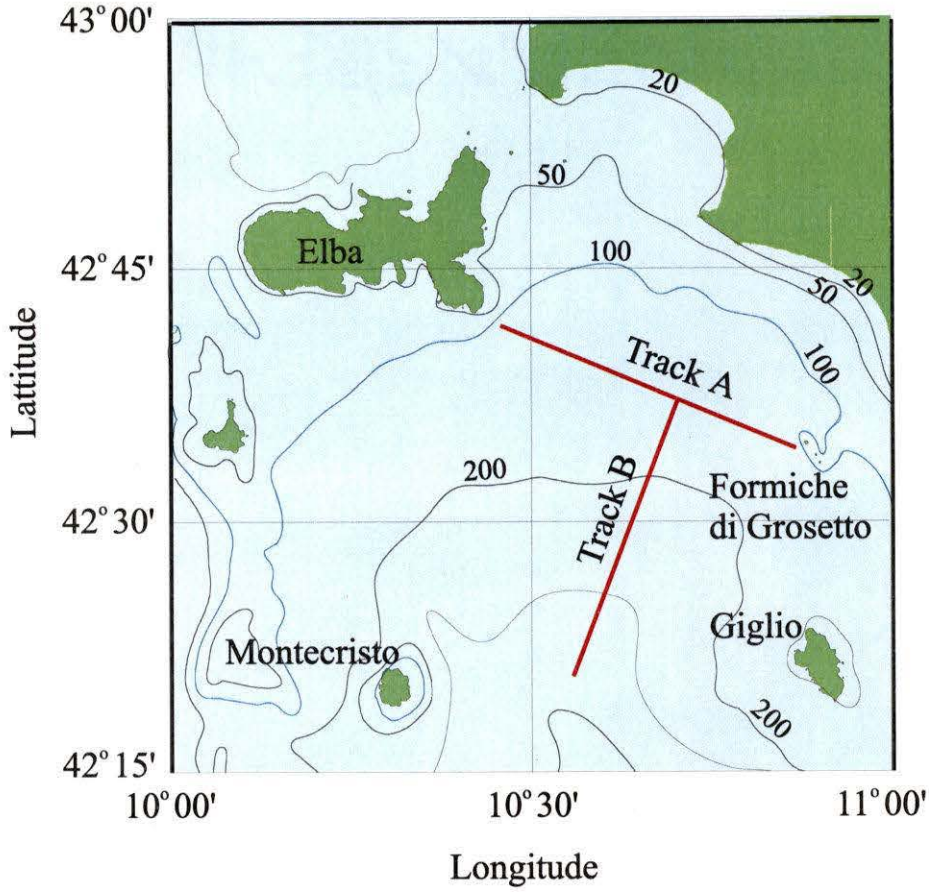

Figure 5.1 South Elba Island experimental site, including ship tracks.

The acoustic data were recorded at two portable hydrophone arrays of fixed configuration and a VLA which was reconfigured depending on the frequency of the source. The acoustic sources consisted of both electrical and explosive devices. The experiment consisted of three parts: towed electrical source and explosive sources deployed over a region of nearly range-independent bathymetry, dropped explosive sources over a region of range-dependent bathymetry, and moored electrical source for time-dependent propagation along a fixed path. The acoustic measurements covered a wide band of frequencies from 50 Hz to 7.5 kHz. The electrical sources produced both linear frequency modulated (LFM) sweeps and continuous wave (CW) signals. In total, these experiments provided a large suite of data.

For this thesis, only a portion of the acoustic data were inverted. The data were recorded on May 18 along track A (see Figs. 5.1 and 5.2). These data were selected because the region was thought to have an almost range-independent bathymetry and because the Elba Island side of the track had a great deal small scale bathymetry variation (Nielsen *et al.* 1998).

The data were recorded using a vertical array of 48 hydrophones (data from one hydrophone were omitted from the analysis because the gain was too low) which spanned from 26–120 m depth with a 2 m spacing between sensors. The source was towed at a depth of about 12 m over a 10-km track, passing within approximately 700 m of the array. The acoustic signal consisted of two LFM sweeps, one from 300–850 Hz and the other from 850–1350 Hz. Figure 5.3 is an example of one of the acoustic signals recorded at the closest point of approach on a mid-water column sensor.

During the recording, a CTD chain was being towed by the source ship and provided accurate sound-speed profiles throughout the experimental area. Bathymetric data were provided by a SWATH multibeam echosounder, which is generally accurate to within approximately 0.5%. However, in this case the SWATH system was not properly calibrated and the measurements are thought to have an absolute uncertainty of approximately 10%. Therefore, the bathymetry is treated as an unknown,

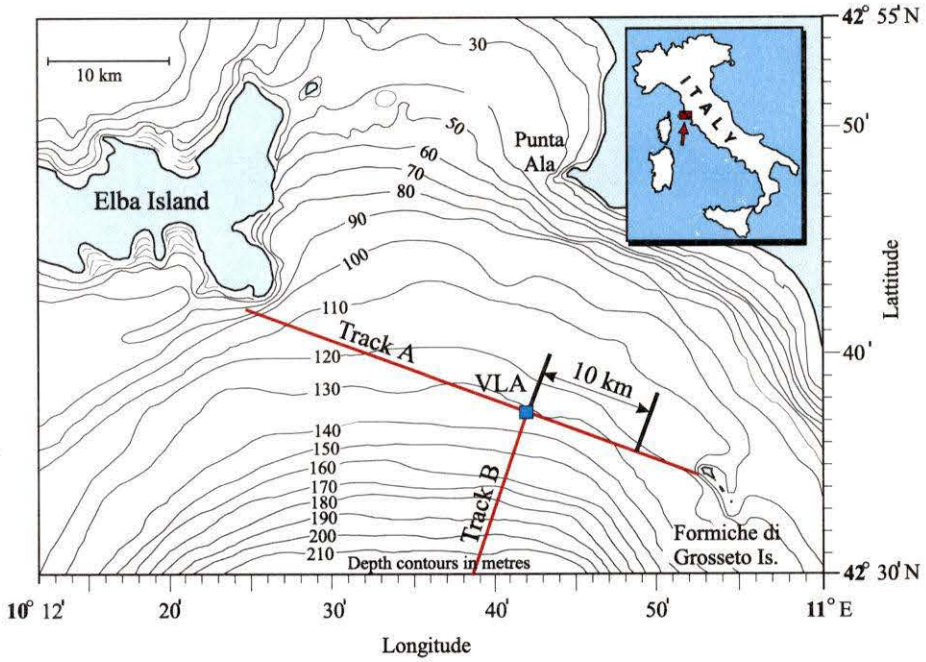

Figure 5.2 Detailed view of the south Elba Island experimental site, including the ship tracks and the 10 km section used in the inversion.

rather than a known parameter in the inversion problem.

5.2 Synthetic Testcases

Before the inversion was applied to the experimental data, synthetic testcases were developed to investigate the different parameter sensitivities and to determine an effective annealing schedule for SSA. The synthetic data were generated using PROSIM (Nielsen *et al.* 1999). To realistically simulate the experimental data, the ocean environment was based on the inversion results from previous experiments conducted in the same region (Hermand and Gerstoft 1996; Siderius and Hermand 1999). Figure 5.4 shows a simple schematic diagram of the ocean environment and gives the parameter values used. In an attempt to conserve computation time, the synthetic cases only made use of the 300–850 Hz band (1 Hz sampling).

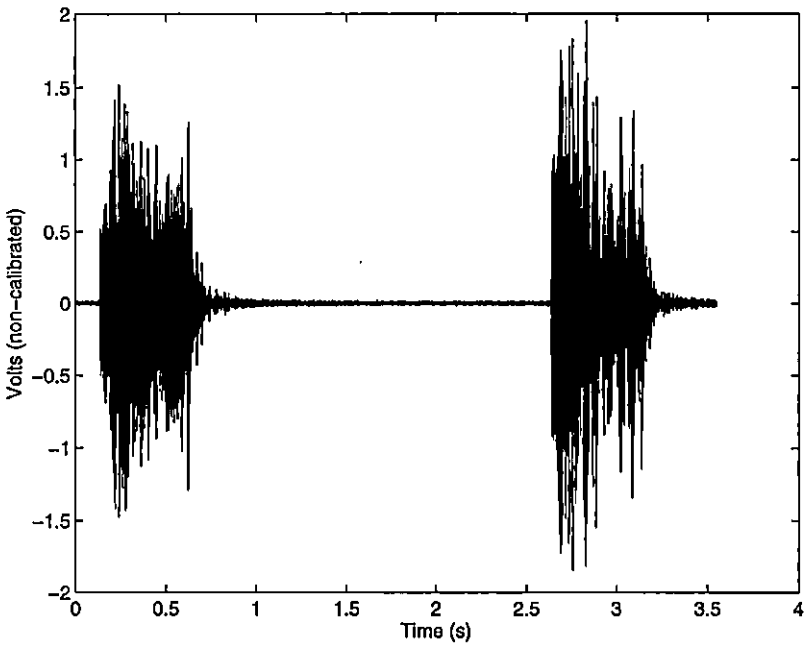

Figure 5.3 Acoustic signal recorded at the closest point of approach on a mid-water column hydrophone.

The SSA algorithm employed the incoherent broadband Bartlett processor (Eq. 2.4) for the inversions. The unknown parameters included in the model were: the water depth D_1, sediment thickness h, sediment compressional speed c_s, basement compressional speed c_b, source range and depth r and z, and the array tilt (measured as a horizontal displacement of the top hydrophone in the plane of propagation while holding the bottom hydrophone fixed). A model consisting of a single sediment layer over a semi-infinite basement was used because the ground truth data suggested the sediment layer was thin (e.g., 3-10 m) (Akal *et al.* 1970; Akal *et al.* 1972; Hermand and Gerstoft 1996; Siderius and Hermand 1999).

Figure 5.5 shows the results of an inversion of noise-free synthetic data. Figure 5.5 (a) shows the mismatch while (b)–(h) shows the convergence of the model parameters with the dotted lines indicating the true parameter values (all models in the simplex are shown). The data appear to be quite sensitive to parameters such as c_b, r, z, and

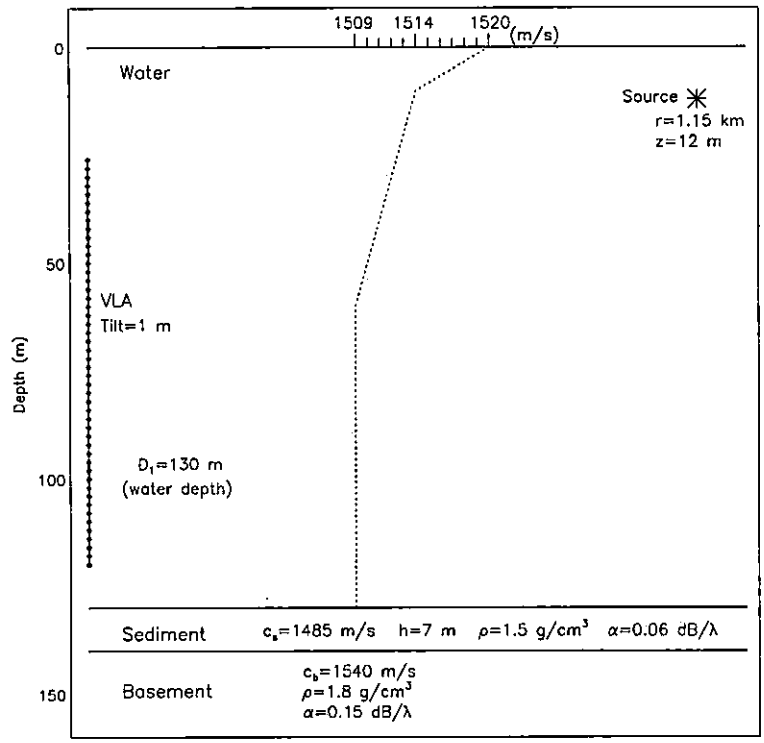

Figure 5.4 Schematic diagram of the synthetic ocean environment used in the inversions.

the array tilt since these parameters lock into their true value early in the inversion. The data are not sensitive to D_1, h and c_s, since even for low mismatches (e.g., $E \approx 10^{-3}$ at temperature step 400–500) the true parameters values are not well resolved.

One problem often associated with geoacoustic inversion is correlated parameters, which can make finding a solution more difficult. Generally, for this type of model (i.e., single sediment layer where the thickness and compressional speed are unknown) a correlation can exist between the sediment thickness and compressional speed. Figure 5.5 (c), (d) could suggest this correlation may exist here since the parameters appear to track each other through the inversion. Also, for this particular inversion another correlation is thought to exist between the water depth and the sediment properties.

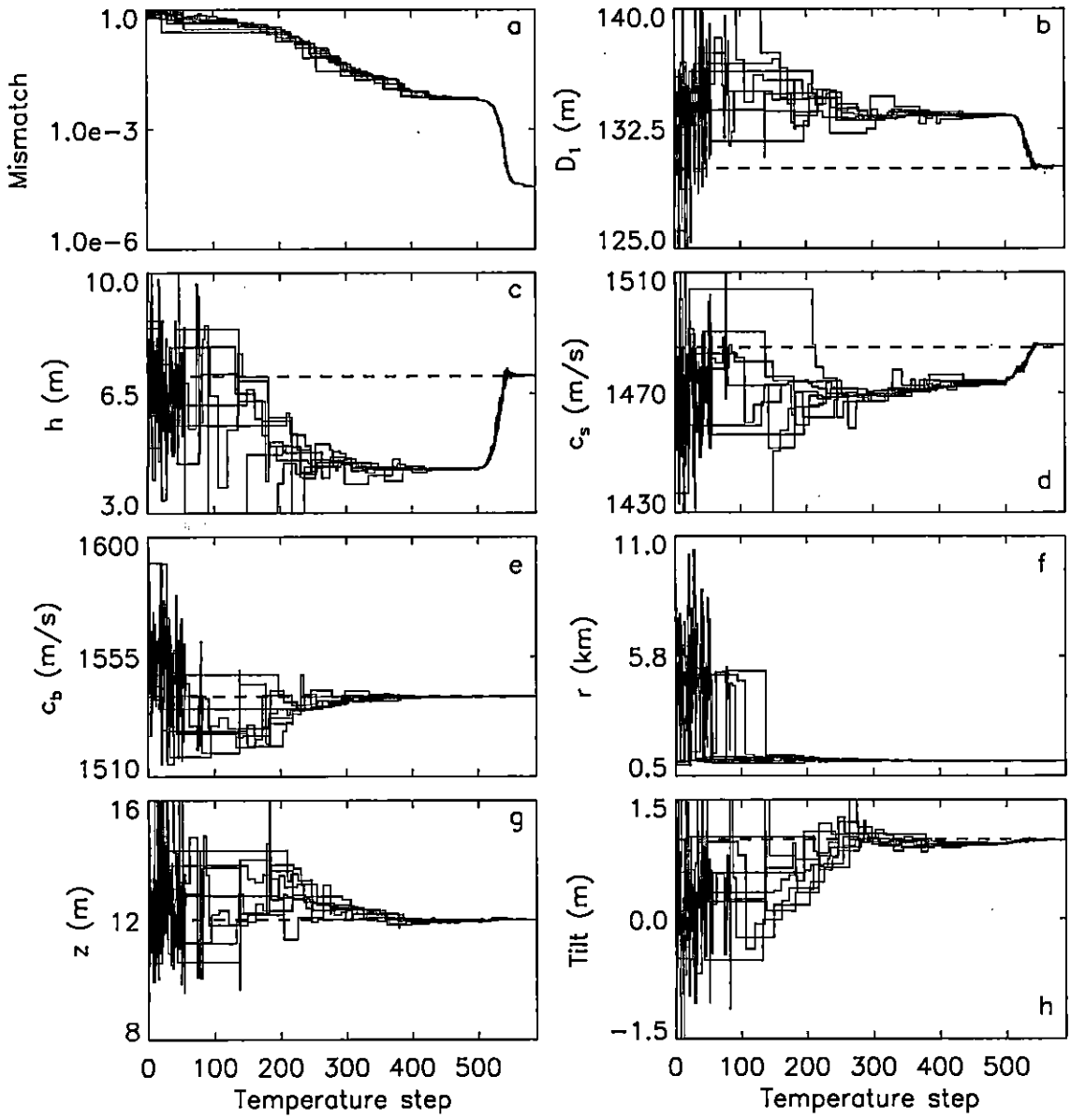

Figure 5.5 The inversion results for a synthetic testcase including the mismatch E and all model parameters. The dashed lines indicate the true parameter values, and the range of ordinate values indicate the search interval.

This correlation arises from the fact that the sediment has a very low compressional speed (i.e., lower than in the water column) and a small attenuation. A trade-off between D_1, h and c_s is created because the sediment layer appears acoustically as part of the water column; therefore, it is difficult to determine accurately these properties.

5.3 Inversion Results

This section describes the inversion of the experimental data. The data used here did not span the entire ship track, but were taken from about 10 km along the tow (see Fig. 5.2). Only the low-frequency sweep (300–850 Hz) in 5 Hz samples was used for the inversions. Using the low-frequency sweep instead of both sweeps lead to more consistent results and required about half as much computation time. Also, using high frequencies can be problematic since experimental and environmental errors (i.e., array position, sound speed in the water column, etc.) have more influence and therefore make the inversion more difficult. Another problem is that at higher frequencies scattering off surface or seabed roughness can begin to effect acoustic propagation.

The range dependence of the bathymetry proved to more important than originally expected (even though the slope was no larger than 0.3°) because the change in water depth corresponded to about three wavelengths at the highest frequency. Therefore, the inversions were carried out using a range-dependent (sloping) bathymetry. PROSIM models a range-dependent bathymetry as a number of discrete range-independent segments. Determining an appropriate number of segments to represent a particular slope is important because using too few segments will not model the slope properly while too many segments wastes computation time.

To determine the correct number of segments for a particular slope, a simple

convergence test was carried out for a 0.25° slope. Ten segments were assumed to be an upper bound for the acceptable number of segments for modeling this slope (previous tests performed comparing PROSIM to other propagation models indicated that for this slope, ten segments were adequate). Figure 5.6 (a)–(c) show examples of a 0.25° slope modeled with two, five and ten segments. Figure 5.6 (d) shows the acoustic pressure (in dB) on a mid-water column hydrophone for all three cases. The results for the two segment case (dotted line) are in relatively poor agreement with the ten segment case (solid line), while the five segment case (dashed line) agrees to an acceptable level of mismatch. The acceptable level was taken to be a Bartlett mismatch of 10^{-3}, since the inversions of real data typically yield mismatches two orders of magnitude greater than this. Therefore, modeling this slope with five segments should be sufficient.

The data were recorded as a set of time series at a VLA. In order to make use of the data, they had to be transformed from the time domain into the frequency domain. The sampling frequency was 3000 Hz, so a 15000-point fast Fourier transform was employed to produce the desired 5-Hz sampling. The absolute signal level was not important (the Bartlett processor normalizes the measured and modeled fields), and therefore the data were transformed without any further processing. The Doppler shift of the towed source was assumed to be negligible because the ship speed was about 2 m/s which leads to a frequency shift shift of about 0.1%. Figure 5.7 shows an example of the power spectrum for an acoustic signal recorded at the closest point of approach on a mid-water column hydrophone.

The range-dependent geoacoustic model used to invert the experimental data had the same form as the range-independent synthetic case described in Chapter 4 (i.e., a single sediment layer over a semi-infinite basement). The exception was that a second water depth was added. The water depths now correspond to values at the source (D_1) and the VLA (D_2). Only the bathymetry was varied with range, all other unknown parameters were assumed to remain constant. The depth and range of the

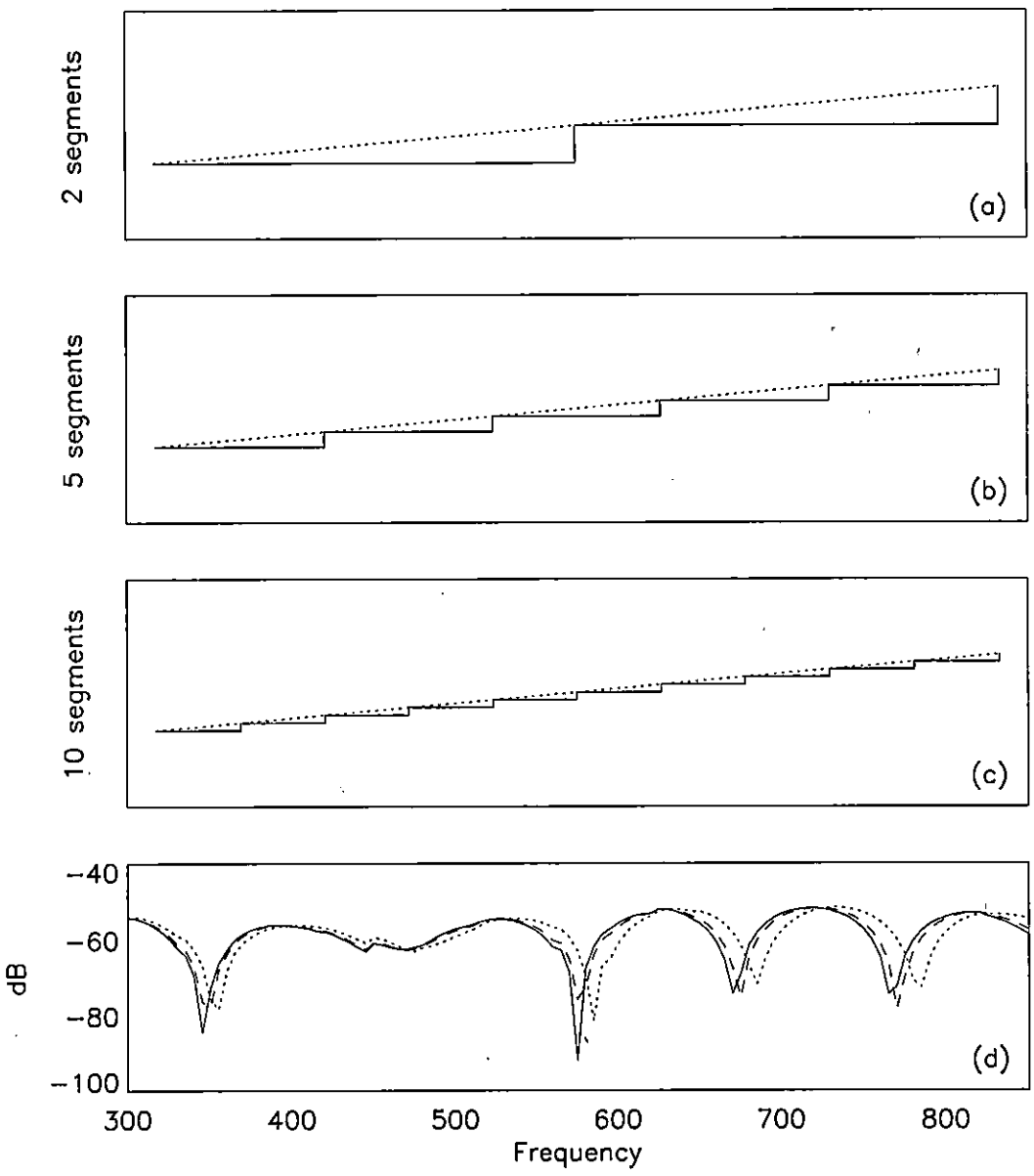

Figure 5.6 Modeling a slope using different numbers of segments (a-c for two, five and ten segments). The acoustic pressure (d) for a mid-water column hydrophone for the two (dotted line), five (dashed line) and ten (solid line) segments. The frequencies are measured in Hz.

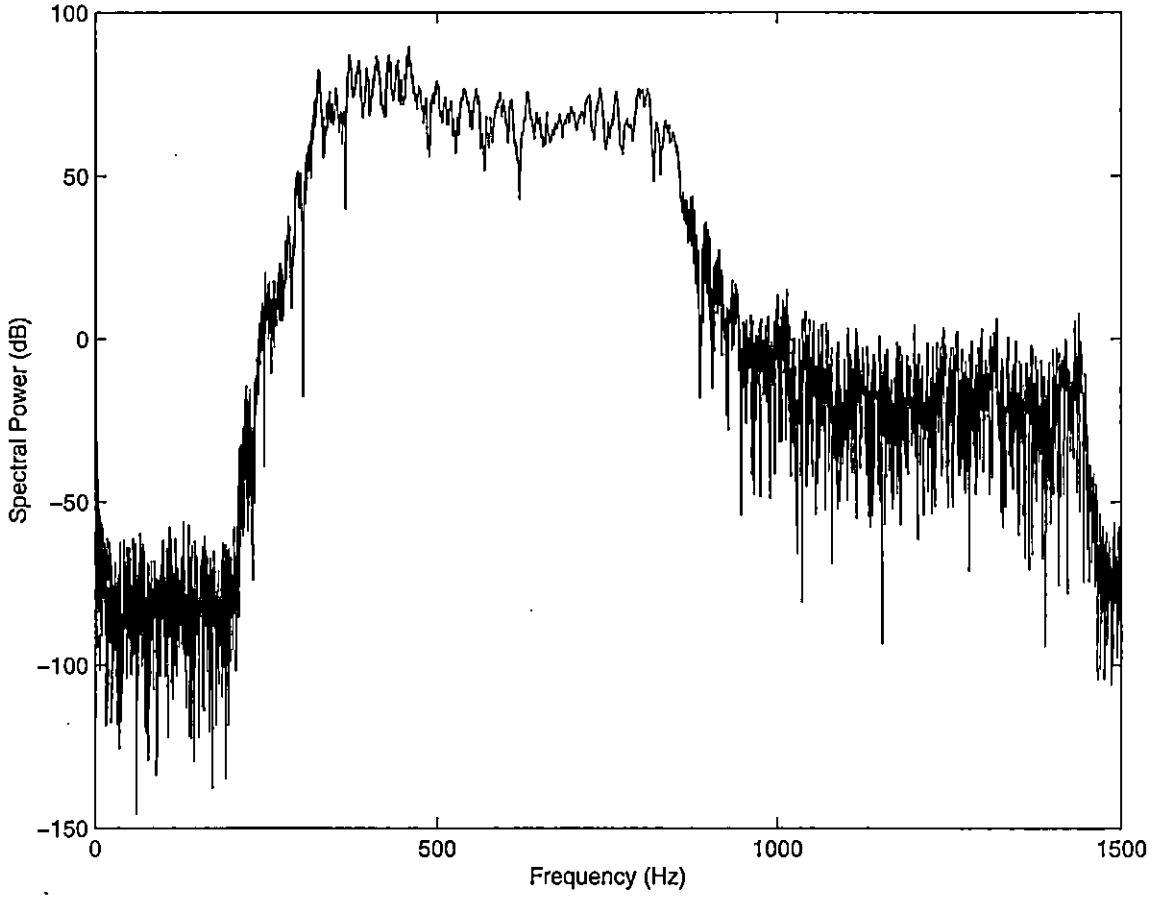

Figure 5.7 Power spectrum for the acoustic signal recorded at the closest point of approach on a mid-water column hydrophone.

Table 5.1 The acoustic signals used in the inversion (time in UTC) and the approximate ranges (km) from the source

095003 / 9.50	102600 / 4.55	105557 / 0.76
095602 / 8.68	103159 / 3.74	105757 / 0.71
100202 / 7.85	103758 / 2.93	105957 / 0.74
100802 / 7.01	104358 / 2.12	110157 / 0.88
101400 / 6.19	104958 / 1.35	110357 / 1.08
102000 / 5.36	105357 / 0.91	——

segments used to define the slope were calculated using D_1, D_2 and r, assuming a linear variation.

The data consisted of recordings of the acoustic signals every two minutes from a source being towed at approximately four knots (see Fig. 5.8). To obtain a detailed description of the environment without inverting all the available data, every third signal was inverted. The exception to this was when the ship was close to the array (from about 700 m to 1000 m) then every signal was inverted. Figure 5.9 shows the approximate range to the source from the VLA as a function of longitude. The ranges were calculated using the approximate VLA position and the Differential Global Positioning System (DGPS) measurements from the ships log.

The closest point of approach was approximately 700 m, which corresponds to the signal recorded at 10:57:57 UTC on May 18. From now on in this thesis, all acoustic signals will be referred to by their time, e.g., the signal recorded at 10:57:57 will be called signal 105757. The tow started close to Formiche di Grosetto, passed by the VLA, and then moved toward Elba Island (see Fig. 5.2). Table 5.1 lists the signals that were inverted and the approximate range from the source to the VLA for each signal.

Multiple SSA inversions were run for each signal and the results (summarized in

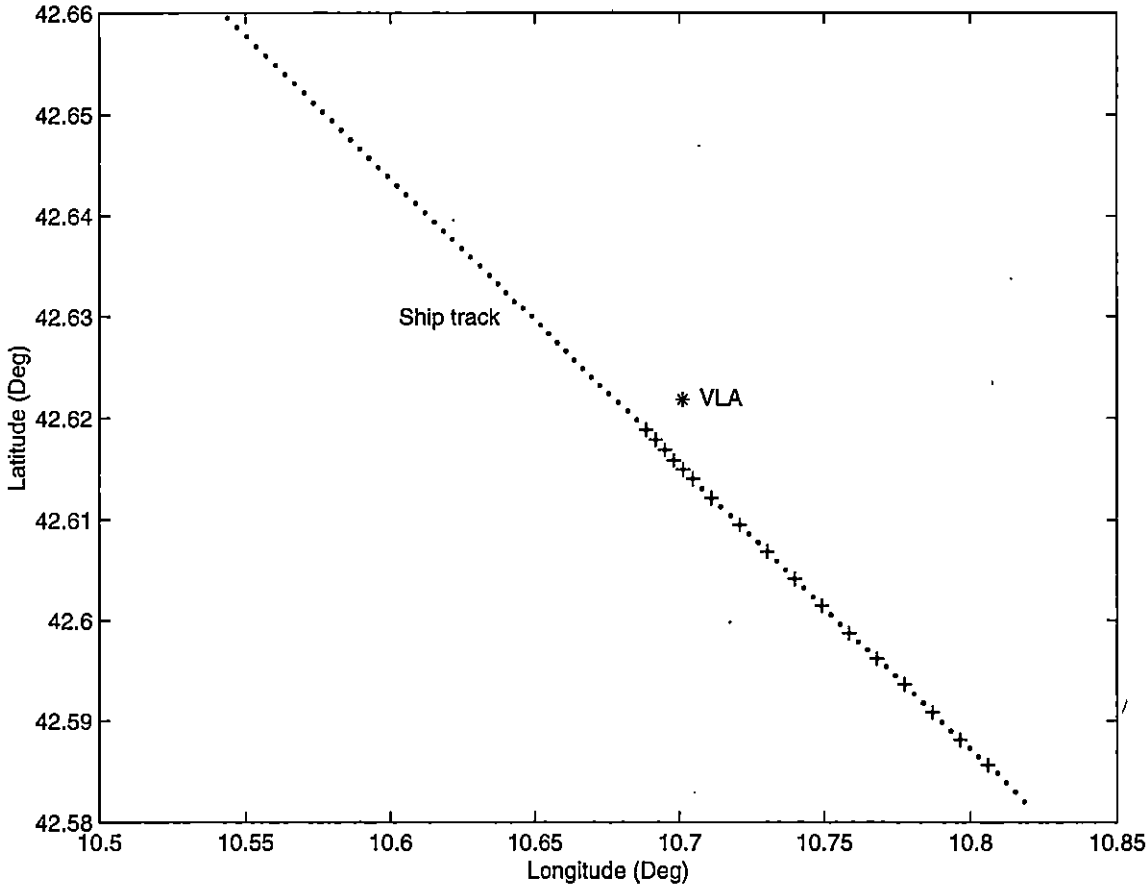

Figure 5.8 Plot of the ship track and the VLA position. The crosses represent the points that were used in the inversions while the dots represent all other points where the source was recorded.

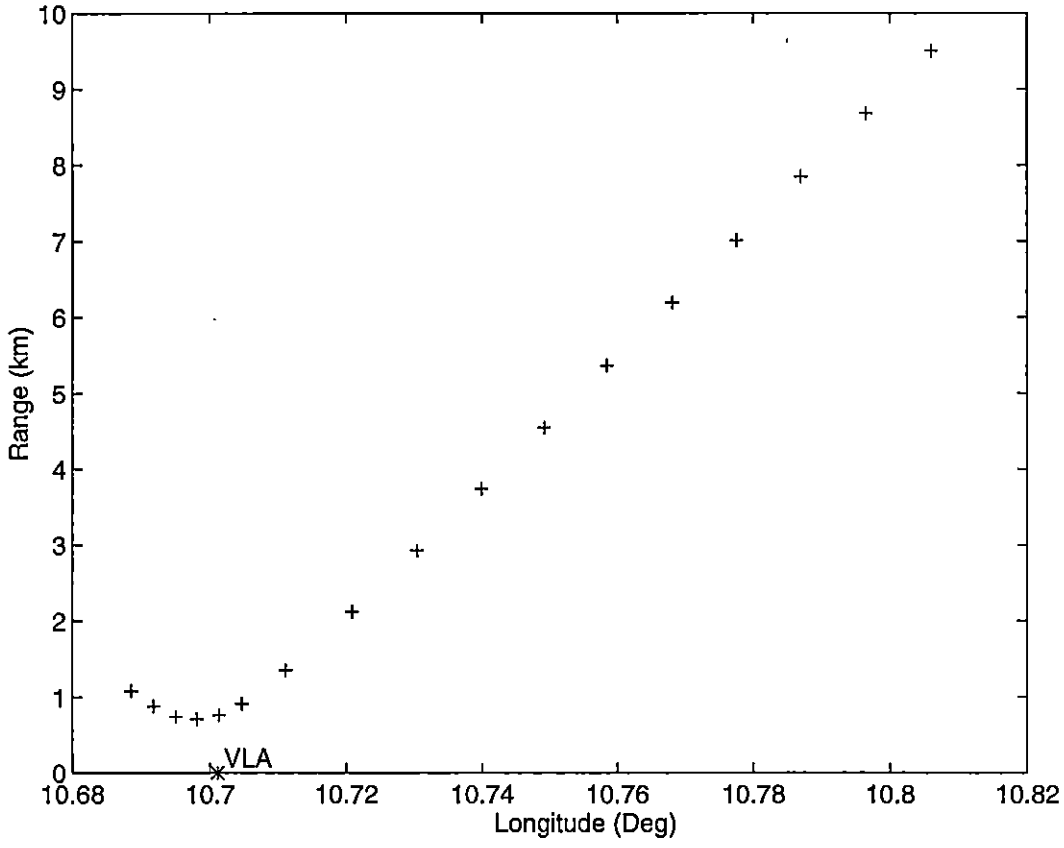

Figure 5.9 The approximate range to the source from the VLA versus longitude.

Fig. 5.10) represent the single inversion that produced the lowest mismatch. Figure 5.10 (a) shows the range from the VLA, with the same orientation as Fig. 5.9, but plotted as a function of inversion number rather than longitude. The dotted line represents the approximate range calculated using the ship track (DGPS) and the VLA position, the crosses (and solid line) indicate the inversion results. The results of the inversion are good, closely tracking the estimated ranges.

Figure 5.10 (b)–(h) show the inversion results for the other unknown parameters plotted in the same fashion as (a). The source depth is shown in Fig. 5.10 (b). The dotted line is the nominal source depth of 12 m. The inversion results are generally good. The slight decrease in source depth at high inversion numbers (i.e., 14–16) does not correspond to a course change or a speed alteration which can cause the source depth to change. This may suggest that for longer ranges the data becomes less sensitive to the source depth.

Figure 5.10 (c) and (d) show the sediment compressional speed and thickness. The compressional-speed results are fairly stable, although there is a small degree of fluctuation. The sediment thickness shows considerably larger fluctuations. Section 5.2 showed that the data were relatively insensitive to both of these parameters, therefore it should not be surprising that there are fluctuations in these results. The dashed lines in Fig. 5.10 correspond to previous inversion results and will be discussed in Sec. 5.4.

The basement compressional-speed results are shown in Fig. 5.10 (e). They appear to very stable. Figure 5.10 (f) is the array tilt which, with the exception of two points, is quite stable. The dotted line is an estimate of the array tilt calculated using the available current data for that period of time. A simple projection of the current vector onto the radial vector between the source and VLA was used to compute this estimate. The estimate has been arbitrarily scaled for comparison since no information was available on how currents affect the array geometry. The inversion results are in good agreement with this tilt estimate.

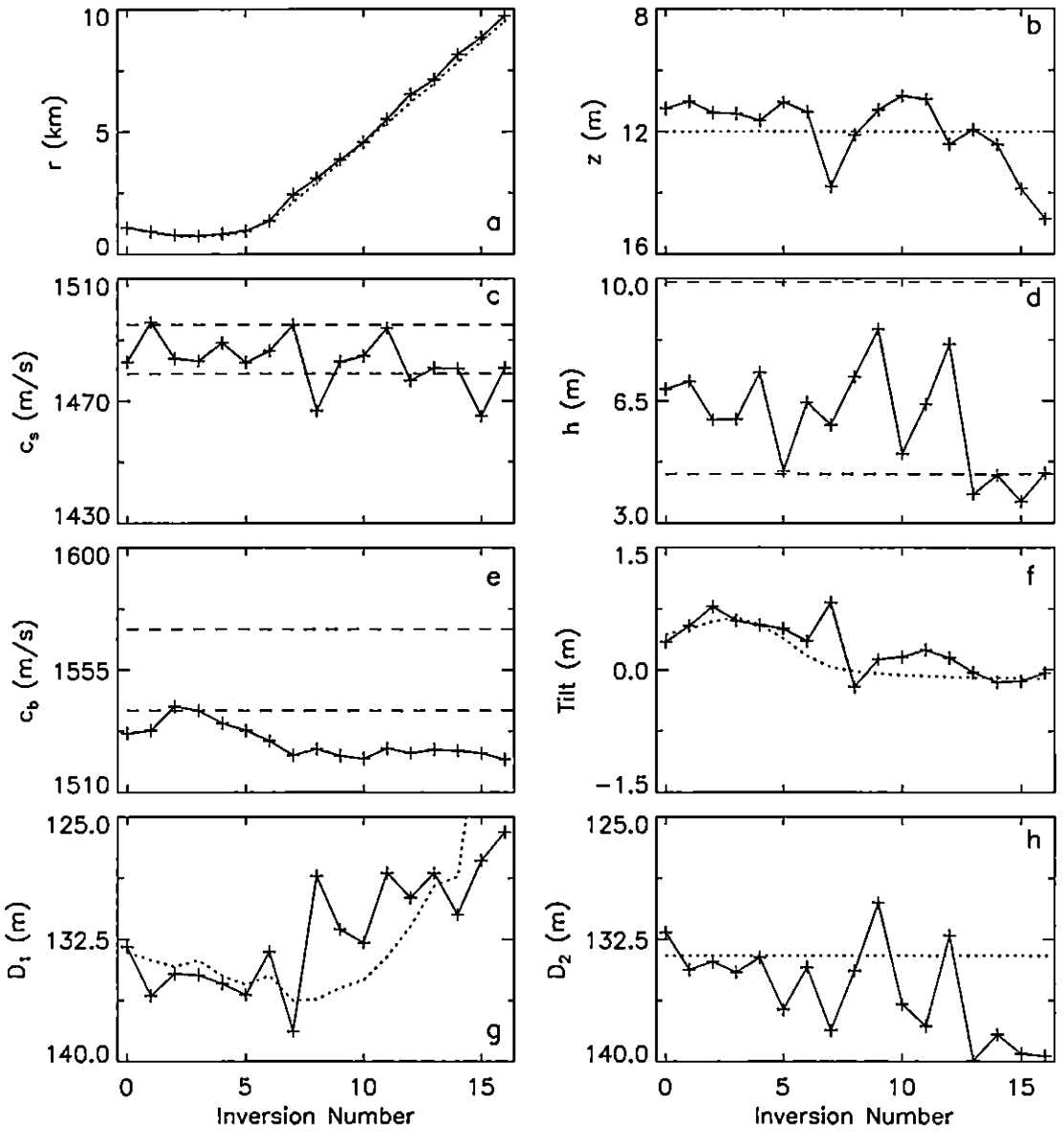

Figure 5.10 Summary of the results of the inversions for r, z, c_s, h, c_b, array tilt, D_1, and D_2. The crosses represent the inversion results. The dotted line represents an estimate of the true values (when information was available). The dashed lines are results from previous inversion experiments (Yellow Shark). The zeroth inversion corresponds to the signal 110357, the signal time decreases as the inversion number increases.

The water depths in Fig. 5.10 (g) and (h) were somewhat difficult to determine reliably, particularly the depth at the VLA, D_2. This parameter should be quite stable because it is the same for each inversion, but as the result in Fig. 5.10 (h) shows, the water depth is not consistent. The dotted line is an estimate of the water depth at the array from three separate echosounder depth measurements. Fig. 5.10 (g) shows the water depth at the source. The dotted line represents the relative water depth estimates from the SWATH data arbitrarily offset because the SWATH system was not calibrated properly (see Sec. 5.1). The dotted line shows that the relative features of the inversion results are in general agreement with the SWATH data.

The inversions in Fig. 5.10 obtained mismatches that ranged from 0.155 to 0.453 with an average mismatch of 0.295. Figure 5.11 shows the mismatch as a function of inversion number.

The inversion of synthetic data in Sec. 5.2 showed that the water depth and the sediment properties were the least sensitive parameters. The results of the experimental data inversions also indicate that theses parameters are the least well resolved. This is likely because a low-speed, low-attenuation sediment layer appears acoustically to be part of the water column, so it is difficult to determine accurately the water depth and sediment properties.

Another source of difficulty in determining sediment properties is the correlations between parameters, especially when the data are not sensitive to these parameters. The inversion of synthetic data suggested that correlations existed between the water depth and the sediment properties. Figure 5.12 illustrates the problem associated with these parameters for signal 102600. In this case c_b, r, z, and the array tilt were held constant at the values found in the inversion and D_1, D_2, c_s, and h were varied over their search intervals. The plots are of the Bartlett function (Eq. 2.4) normalized to one with respect to the different parameters. Figure 5.12 (a)–(c) shows that D_1 is the least sensitive of these four parameters. In each case, D_1 is relatively uncorrelated with respect to the other parameters and therefore does not have as much of an effect

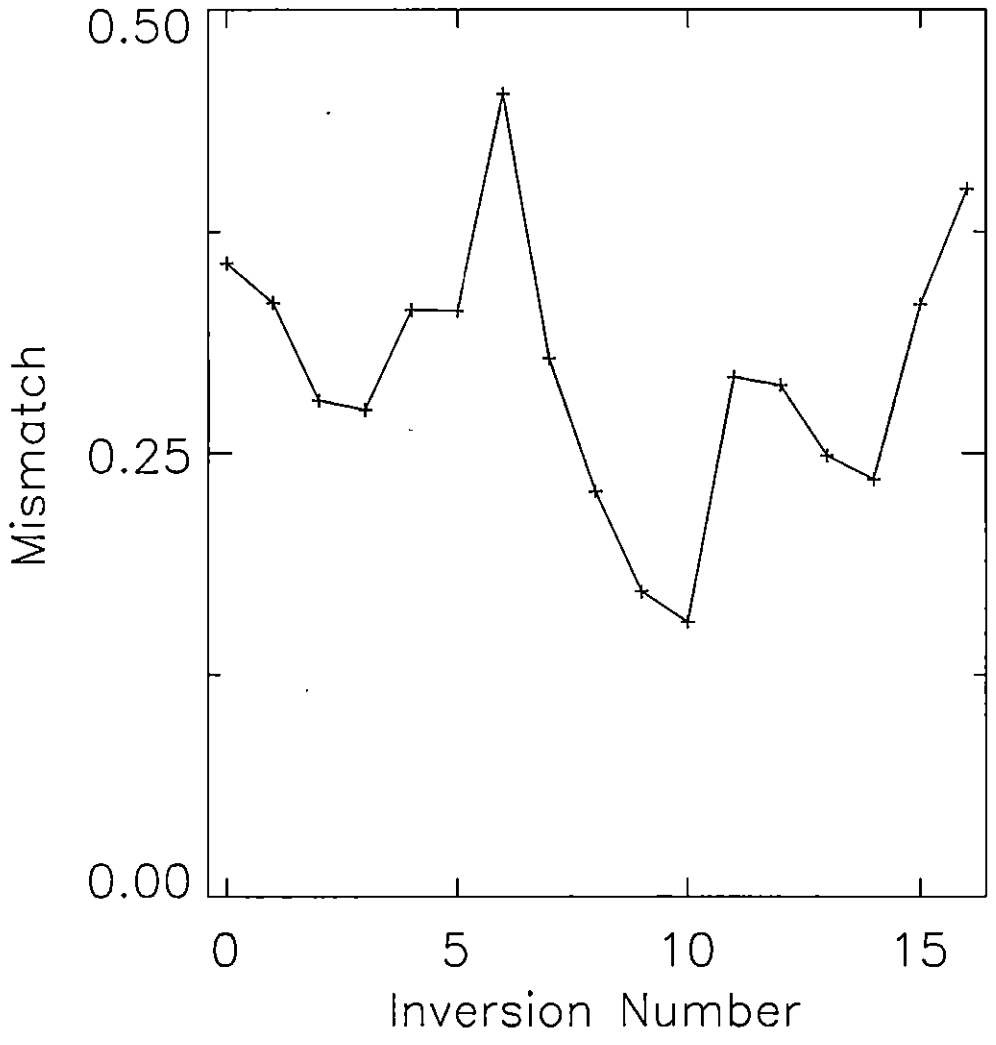

Figure 5.11 The mismatch as a function of inversion number for the experimental data.

on the objective function. Figure 5.12 (d)–(f) show strong correlations between D_2, c_s and h (i.e., narrow valleys not aligned with the parameter axes). Therefore, these paramteres can vary over a large range (almost the entire search interval for Fig. 5.12 d) and produce essentially the same level of mismatch.

Once all the inversion results were collected, a comparison of the measured and modeled pressure fields was carried out. For the measured field the source characteristics, including source level, were taken out. Figure 5.13 shows the pressure fields for signals 102600 and 105557, normalized in 5 Hz bands as in the Bartlett processor. These particular signals were chosen because they represent the upper and lower levels of mismatch and they are also from very different ranges. For signal 102600 (mismatch $E = 0.155$, and range $r \approx 4.5$ km) the fields are in good agreement. Even smaller scale structure such as the circular regions of high intensity at low frequencies and shallow depths (i.e., 300–500 Hz, 26–60 m depth) are seen in both plots.

Signal 105557 is a little more complicated. The inversion attained a mismatch of 0.331 and produced a source range of 0.85 km. At this close range the evanescent modes are still important to the acoustic field because they have not been attenuated. These modes are responsible for most of the fine-scale structure. PROSIM does not use the evanescent modes when computing the acoustic fields and therefore is not able to reproduce all of the fine scale structure. Thus, only the larger-scale structure (e.g., regions of high and low intensity) should be similar in the two fields. This is clearly evident in Fig. 5.13. Figure 5.14 illustrates the difference when the evanescent modes are included. ORCA was used to replicate signal 105557 for different frequencies in the band. In each case, the pressure was computed with and without the evanescent modes. The dotted line in Fig. 5.14 represents the pressures computed without the evanescent modes. For each frequency, the pressure computed without the evanescent modes has less fine-scale structure then the pressure computed with the evanescent modes.

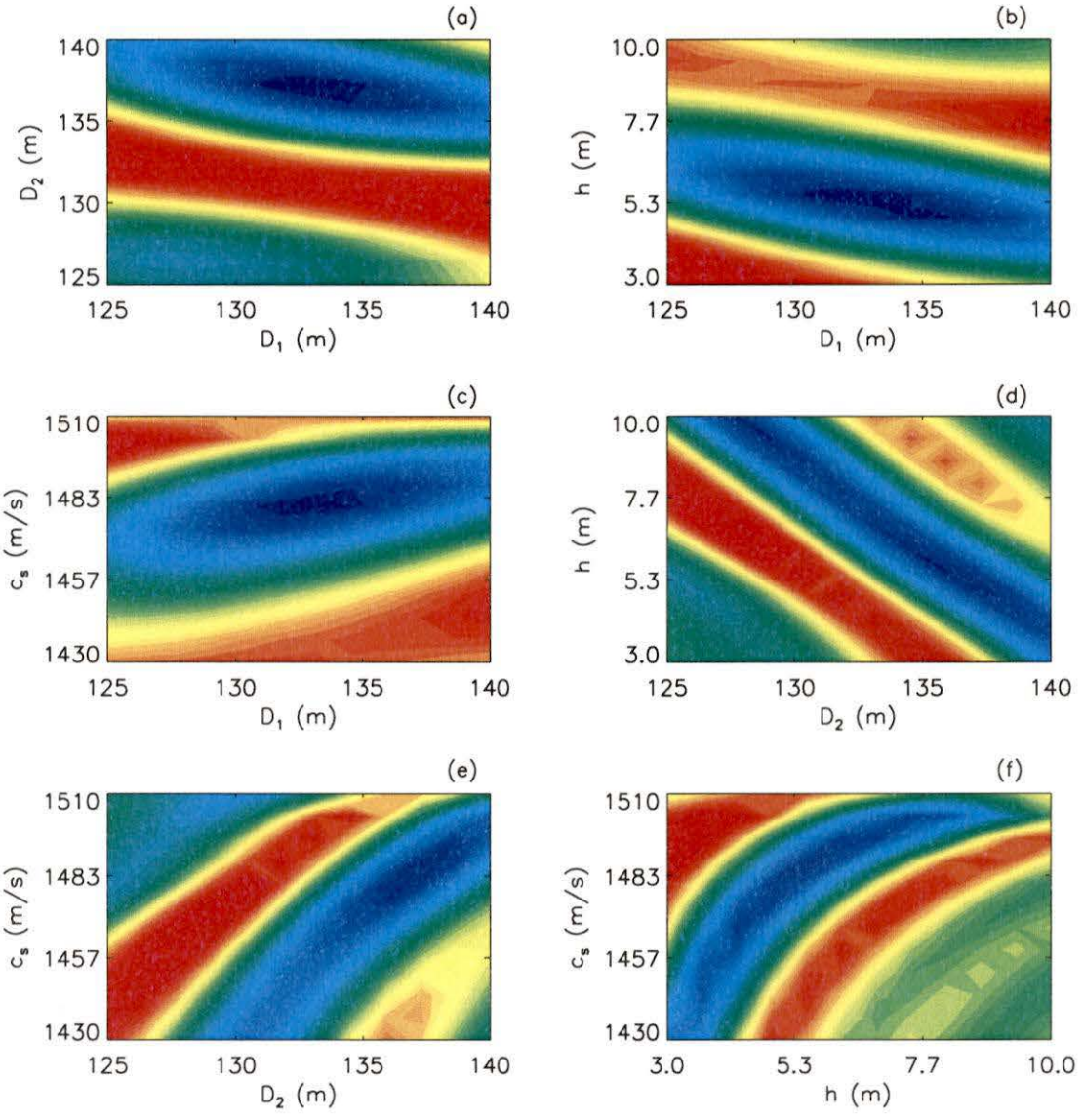

Figure 5.12 Mismatch as a function of D_1, D_2, h, and c_s for signal 102600, illustrating correlations that exist between the parameters. Blue represent low mismatch, while red represent high.

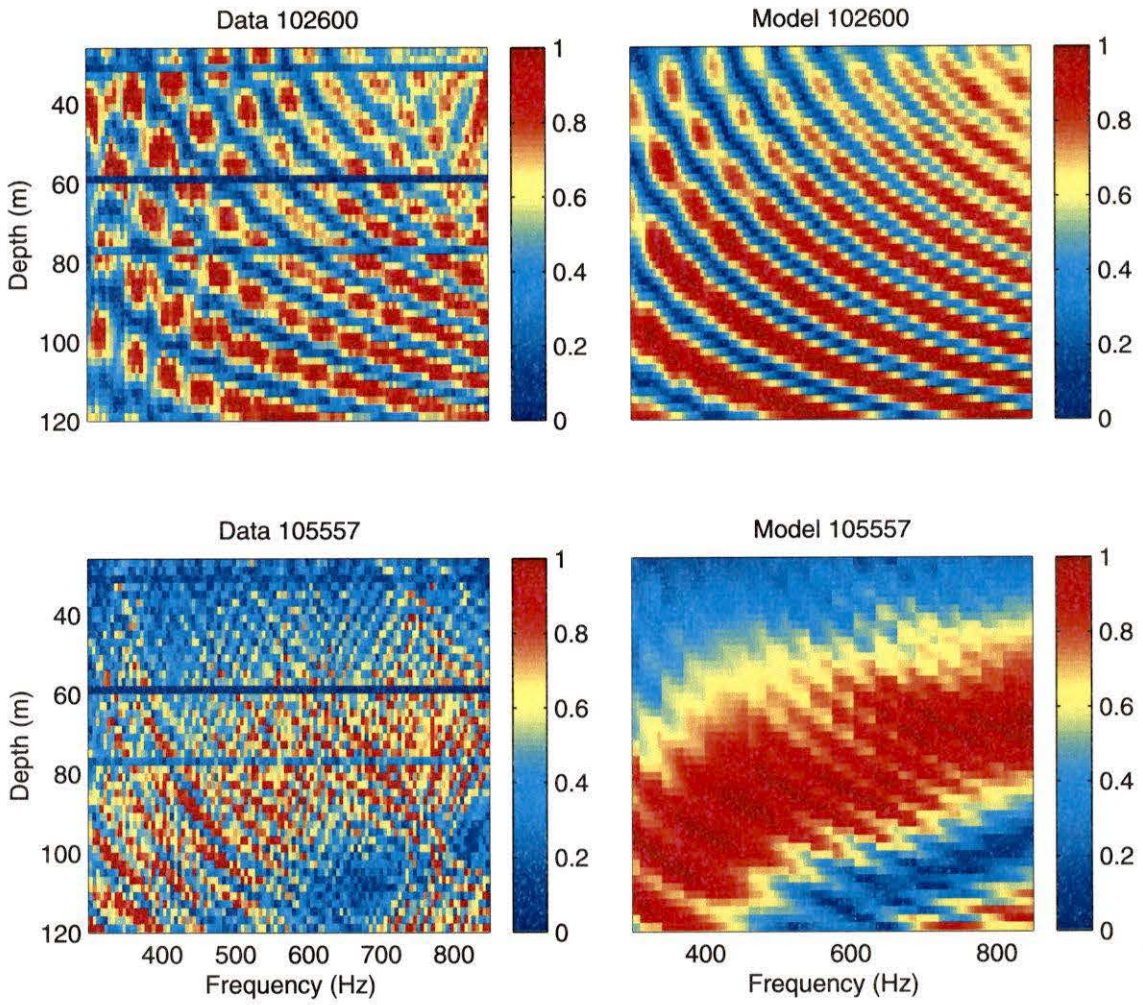

Figure 5.13 Measured and modeled pressure fields for two signals 102600 and 105557. The source characteristics have been taken out and the fields have been normalized in 5 Hz bands. The channel at 60 m depth was omitted from the inversion due to low gain.

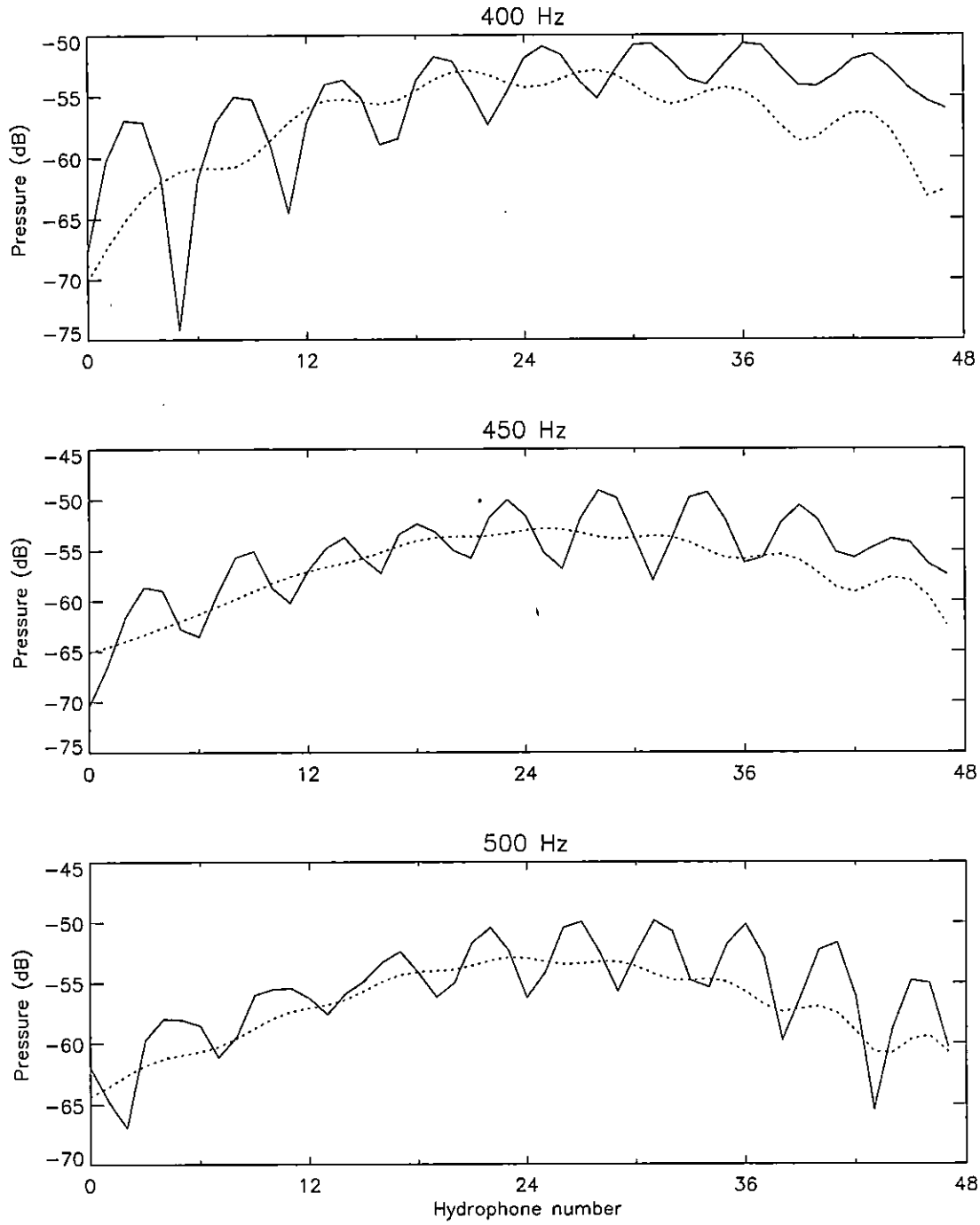

Figure 5.14 ORCA generated pressures for three different frequencies in the band. In each case the dotted lines are the pressure computed without the evanescent modes.

5.4 Comparison to Past Inversions

The Yellow Shark experiments (Hermand and Gerstoft 1996; Siderius and Hermand 1999) were conducted in the same region as the PROSIM'97 experiment. For both experiments, inversions were carried out to determine the geoacoustic properties of the region. Hermand and Gerstoft (1996) carried out a GA inversion of broadband data. Siderius and Hermand (1998) inverted sparse array broad band transmission loss data using a simple forward modeling technique. Since the the Yellow Shark and PROSIM'97 experiments were conducted in the same region (but not along the same track) it is reasonable to expect the seabed properties (sediment thickness and sediment and basement compressional speeds) to be similar. This provides a further check of the PROSIM'97 inversion results obtained here.

The results of the two Yellow Shark experiments and the PROSIM'97 experiment are summarized in Table 5.2. Figure 5.10 shows the SSA inversion results for the PROSIM'97 data and the results of the Yellow Shark experiments. In Fig. 5.10 (c)–(e) the dashed lines represent the average results for each of the two Yellow Shark experiments. For the sediment compressional speed (Fig. 5.10 c), the PROSIM'97 inversion results are close to the Yellow Shark results. For the sediment thickness (Fig. 5.10 d), the PROSIM'97 results were in between the two Yellow Shark results (4.5 m and 10 m). Finally, the PROSIM'97 inversion is in good agreement with Hermand and Gerstoft's (1996) result (1540 m/s) for the basement compressional speed (Fig. 5.10 e) but it is lower than Siderius and Hermand's (1998) result of 1570 m/s.

Overall, the results of the PROSIM'97 inversion are in good agreement with the available ground truth data and the Yellow Shark inversion results, despite the fact that the various experiments were conducted at different times of the year and the analysis were carried out using different inversion techniques and forward models.

These results offer encouragement that broadband MFP methods can provide meaningful estimates of the true geoacoustic properties.

Table 5.2 The results for h, c_s and c_b for the three different inversion experiments conducted in the Elba Island area. YS1 corresponds to Hermand and Gerstoft's (1996) results, YS2 corresponds to Siderius and Hermand's (1998) results and PRO represents the PROSIM'97 inversion results.

Experiment		h (m)	c_s (m/s)	c_b (m/s)
PRO	Min	3.6	1465	1522
	Max	8.6	1496	1542
	Ave	6	1483	1529
YS1	Min	5	1465	1520
	Max	15	1525	1560
	Ave	10	1495	1540
YS2	Min	3.1	1463	1551
	Max	5.6	1493	1586
	Ave	4.4	1479	1570

Chapter 6

Conclusion

Recently, a lot of attention has been given to geoacoustic inversion including the development of algorithms and forward models. The Workshop97 (Tolstoy *et al.* 1998) was set up particularly for testing the different algorithms and models. In this thesis, a new algorithm for geoacoustic inversion was developed, validated, and applied to experimental data.

SSA is a hybrid inversion algorithm that incorporates a local component based on the DHS method into a global fast SA algorithm. DHS is based on an intuitive geometric scheme for moving downhill in parameter space without computing partial derivatives or solving systems of equations. SA uses an analogy to the physical process of annealing to search the parameter space. DHS and SA were chosen for the hybrid inversion algorithm because of their inherent simplicity and efficiency, and because the resulting algorithm retains a memory of good regions of the parameter space.

SSA was validated using noise-free synthetic data for the Workshop97 benchmark testcases. In total, 13 different testcases were evaluated, 12 where the form of the geoacoustic model was known (i.e., a single sediment layer over a semi-infinite basement), and one where the model form (a general geoacoustic profile) was included as part of the inversion. When the form of the geoacoustic model was known, SSA produced excellent estimates for all the unknown parameters with the exception of the basement density and attenuation in a few cases. In general, the data are not sensitive to these parameters, so it is not surprising that they were sometimes poorly resolved. For the general geoacoustic profile, an under-parameterized approach was employed to determine the model which achieved the best trade-off between low mismatch and a simple structure. The SSA algorithm produced a good, if somewhat

simplified, approximation to the true compressional speed and density profiles.

A comparison of SSA with DHS and SA was carried out using both a workshop testcase and a multimodal function. In each case, SSA performed as well or better then DHS and SA, and required far fewer forward model (or function) evaluations, resulting in computation times that were at least an order of magnitude smaller.

The SSA algorithm was also applied to acoustic data recorded in the Mediterranean Sea near Elba Island off the west coast of Italy. This area was chosen because previous experiments had been conducted there and therefore a good deal of ground truth information was available. The data consisted of time series recorded at a vertical array of 48 hydrophones due to a towed acoustic source which produced many different signals. For this work, LFM sweeps from 300-850 Hz were used.

A SSA inversion was carried out to determine geoacoustic and geometric properties of the ocean environment. The results for all parameters except the water depths were reasonably well resolved. Parameters such as the source range and depth and the array tilt were in good agreement with the available ground truth data. The sediment and basement parameters were in reasonable agreement with inversion results from previous experiments in the region. The water depth at the source was generally in agreement with the measured bathymetry along the source track. The water depth VLA was poorly determined with a wide range of values being determined.

The experimental area is known to be characterized by a thin sediment layer with a low compressional speed and a low attenuation. Therefore this layer appears to be acoustically part of the water column, which leads to several problems in geoacoustic inversion. First, the data are not sensitive to the water depth or the sediment properties, and secondly correlations between the water depth and sediment properties exist. These problems likely led to the trouble with resolving the water depths.

In this thesis, SSA has proven to be an effective algorithm for geoacoustic inversion. SSA also proved to very effective at inverting a known multimodal function. For synthetic testcases it easily outperformed DHS and SA producing as good or better

results in a fraction of the time. SSA was also successful at inverting difficult experimental data producing results that were in agreement with the available ground truth data and the inversion results of previous experiments. Hence, SSA would seem to be a very useful approach to solving the geoacoustic inversion problem.

M. R. Fallat

References

Akal, T.
Bathymetry and bottom structure of zones near the Island of Elba used for acoustic trials in shallow water, *SACLANTCEN Technical Memorandum No. 162* SACLANT Undersea Research Centre, La Spezia, Italy (1970).

Akal, T., Gehin, C., Matteucci, B., and Tonarelli, B.
Measured and computed physical properties of sediment cores: Island of Elba zone, *SM-82*, SACLANT Undersea Research Centre, La Spezia, Italy (1972).

Chunduru, R.K., Sen, M.K., and Stoffa, P.L.
Hybrid optimization methods for geophysical inversion, *Geophysics*, **62**, 1196–1207, 1997.

Collins, M.D., Kuperman, W.A., and Schmidt, H.
Nonlinear inversion for ocean-bottom properties, *Journal of the Acoustical Society of America*, **92**, 2770–2783, 1992.

Collins, M.D. and Fishman, L.
Efficient navigation of parameter landscapes, *Journal of the Acoustical Society of America*, **98**, 1637–1644, 1995.

Constable, S.C., Parker, R.L. and Constable, C.G.
A practical algorithm for generating smooth models from electromagnetic sounding data, *Geophysics*, **52**, 289-300, 1987.

Dosso, S.E., Yeremy, M.L., Ozard, J.M., and Chapman, N.R.
Estimation of ocean-bottom properties by matched-field inversion of acoustic field data, *IEEE Journal of Oceanic Engineering*, **18**, 232–239, 1993.

Dosso, S.E., Ozard, J.M., and Fawcett, J.A.
Inversion of acoustic field data for bathymetry and bottom sound speed via simulated annealing, *Acoustic Signal Processing*, edited by J.M.F. Moura and I.M.G. Lourtie, pp. 232–239, Kluwer Academic Publishers, Netherlands, 1993.

Dosso, S.E. and Sotirin, B.J.
Optimal array element localization, Submitted to *Journal of the Acoustical Society of America*, 1998.

Fallat, M.R. and Dosso, S.E.
Geoacoustic inversion for the Workshop97 benchmark test cases using simulated annealing, *Journal of Computational Acoustics*, **6**, 29–43, 1998.

Fallat, M.R. and Dosso, S.E.
Geoacoustic inversion via local, global and hybrid inversion, *Journal of the Acoustical Society of America*, Accepted, 1999.

Fallat, M.R., Nielsen, P.L. and Jensen, F.B.
Geo-acoustic inversion of the PROSIM'97 experimental data using simplex simulated annealing, SACLANT Undersea Research Centre, La Spezia, Italy (1999).

Gerstoft, P.
Inversion of seismoacoustic data using genetic algorithms and *a posteriori* probability distributions, *Journal of the Acoustical Society of America*, **95**, 770–782, 1994.

Gerstoft, P.
Inversion of acoustic data using a combination of genetic algorithms and the Gauss-Newton approach, *Journal of the Acoustical Society of America*, **97**, 2181–2190, 1995.

Hermand, J.-P. and Gerstoft, P.
Inversion of broad-band multitone acoustic data from the YELLOW SHARK summer experiments, *IEEE Journal of Oceanic Engineering*, **21**, 324–346, 1996.

Jensen, F.B., Kuperman, W.A., Porter, M.B. and Schmidt, H.
Computational ocean acoustics, AIP Press, New York, 1994.

Kirkpatrick, S., Gelatt, C.D.Jr. and Vecchi, M.P.
Optimization by simulated annealing, *Science*, **220**, 671–680, 1983.

Lane, F.
Estimation of the kinematic rupture parameters from historical seismograms: An application of simulated annealing to a non-linear optimization problem, Ph.D. Thesis, Colorado School of Mines, Golden, Colorado, 1992.

Lindsay, C.E. and Chapman, N.R.
Matched field inversion for geoacoustic model parameters using adaptive simulated annealing, *IEEE Journal of Oceanic Engineering*, **18**, 224–231, 1993.

Liu, P., Hartzell, S. and Stephenson, W.
Non-linear multiparameter inversion using a hybrid global search algorithm: Applications in reflection seismology, *Geophysics Journal International*, **122**, 991–100, 1995.

Menke, W.
Geophysical data analysis: Discrete inverse theory, Academic Press, New York, 1984.

Musil, M.
Range-dependent matched-field inversion using the downhill simplex algorithm, M.Sc. Thesis, University of Victoria, Victoria, B.C. Canada, 1998.

Nelder, J.A. and Mead, R.
A simplex method for function minimization, *Computer Journal*, **7**, 308–311, 1965.

Nielsen, P.L., Jensen, F.B., and Bini-Verona, F.
Environment and acoustic data collected in the South Elba during the PROSIM'97 experiment, *SACLANTCEN Internal document*, SACLANT Undersea Research Centre, La Spezia, Italy (1998).

Nielsen, P.L., Bini-Verona, F. and Jensen, F.B.
PROSIM User Manual, SACLANT Undersea Research Centre, La Spezia, Italy (1999).

Pierce, A.D. Extension of the method of normal modes to sound propagation in an almost-stratified medium, *Journal of the Acoustical Society of America*, **37**, 19–27, 1965.

Press, W.H., Teukolsky, S.A., Vetterling, W.T., and Flannery, B.P.
Numerical recipes in FORTRAN, pp. 387–448, Cambridge University Press, Cambridge, 1992.

Rajan, S.D, Lynch, J.F., and Frisk, G.V.
Perturbative inversion methods for obtaining bottom geoacoustic parameters in shallow water, *Journal of the Acoustical Society of America*, **82**, 998–1017, 1987.

Schmidt, H.
SAFARI: Seismo-acoustic fast field algorithm for range-independent environments, *Rep. SR-113*, SACLANT Undersea Research Centre, La Spezia, Italy (1988).

Sen, M.K. and Stoffa, P.L.
Global optimization methods in geophysical inversion, Elsevier Scientific Publishers B.*(v)* . Amsterdam, 1995.

Siderius, M. and Hermand, J.-P.
Yellow Shark Spring 95: Inversion results from sparse broad-band acoustic measurements over a highly range dependent soft clay layer, *IEEE Journal of Oceanic Engineering*, In Press 1999.

Szu, H. and Hartley, R.
Fast simulated annealing, *Physics Letters A*, **122**, 157–162, 1987.

Tarantola, A.
Inverse problem theory: Methods for data fitting and model parameter estimation , Elsevier Scientific Publishers B.V., Amsterdam, 1987.

Tolstoy, A.L.
Matched-field processing for underwater acoustics , World Scientific Publishing, Singapore, 1993.

Tolstoy, A.L., Chapman, N.R. and Brooke, G.
Workshop97: Benchmarking for geoacoustic inversion in shallow water, *Journal of Computational Acoustics*, **6**, 1–28, 1998.

Westwood, E.K., Tindle, C.T., and Chapman, N.R.
A normal mode model for acousto-elastic ocean environments, *Journal of the Acoustical Society of America*, **100**, 3631–3645, 1996.

Zala, C.A. and Ozard J.M.
Estimation of geoacoustic parameters from narrowband data using a search-optimization technique, *Journal of Computational Acoustics*, **6**, 223–245, 1998.

Appendix A

Comparison using a multimodal function

To provide a further comparison of SSA with DHS and SA, all three algorithms were applied to multimodal function. The function considered is a version of that used by Musil (1998) extended to higher dimensions:

$$E(x_1, x_2, x_3, x_4, x_5, x_6) = 4.8 + x_1^2 + 5x_2^2 + 0.1x_3^2 + 0.05x_4^2 + x_5^2 + x_6^2 - 0.3\cos 4\pi(x_1 - x_2) - 1.4\cos 4\pi(x_1 + x_2) - 0.5\cos 10\pi(0.05x_4 - 0.1x_3) - 1.0\cos 10\pi(0.05x_4 + 0.1x_3) - 0.25\cos 5\pi(x_5 - x_6) - 1.35\cos 5\pi(x_5 + x_6). \quad (A.1)$$

The function (A.1) has three important features: a large number of local minima, correlations between parameters, and a range of parameter sensitivities. Figure A.1 shows the function in one and two dimensions. The global minimum of the function is $E(x_i) = 0$ which occurs at the origin (i.e., $x_i = 0, i = 1, ..., 6$). Two criteria were adopted to define a successful inversion. The first criterion is that the model parameters closely approximate their values at the global minima (i.e., $x_i \leq 10^{-3}, i = 1, ..., 6$). The second criterion is that a low function value is obtained (i.e., $E \leq 10^{-5}$).

The DHS method was started from 5000 random starting points. Figure A.2 shows the results of the 5000 independent runs. For this case, 8% of the parameter values were within $x_i \leq 10^{-3}$ and 1% of the solutions achieved $E \leq 10^{-5}$. The same set of convergence criteria that were used in Sec. 4.3 were employed here.

For both SA and SSA, 100 independent runs were performed in order to better asses their effectiveness for this problem. The annealing schedule for SA consisted of

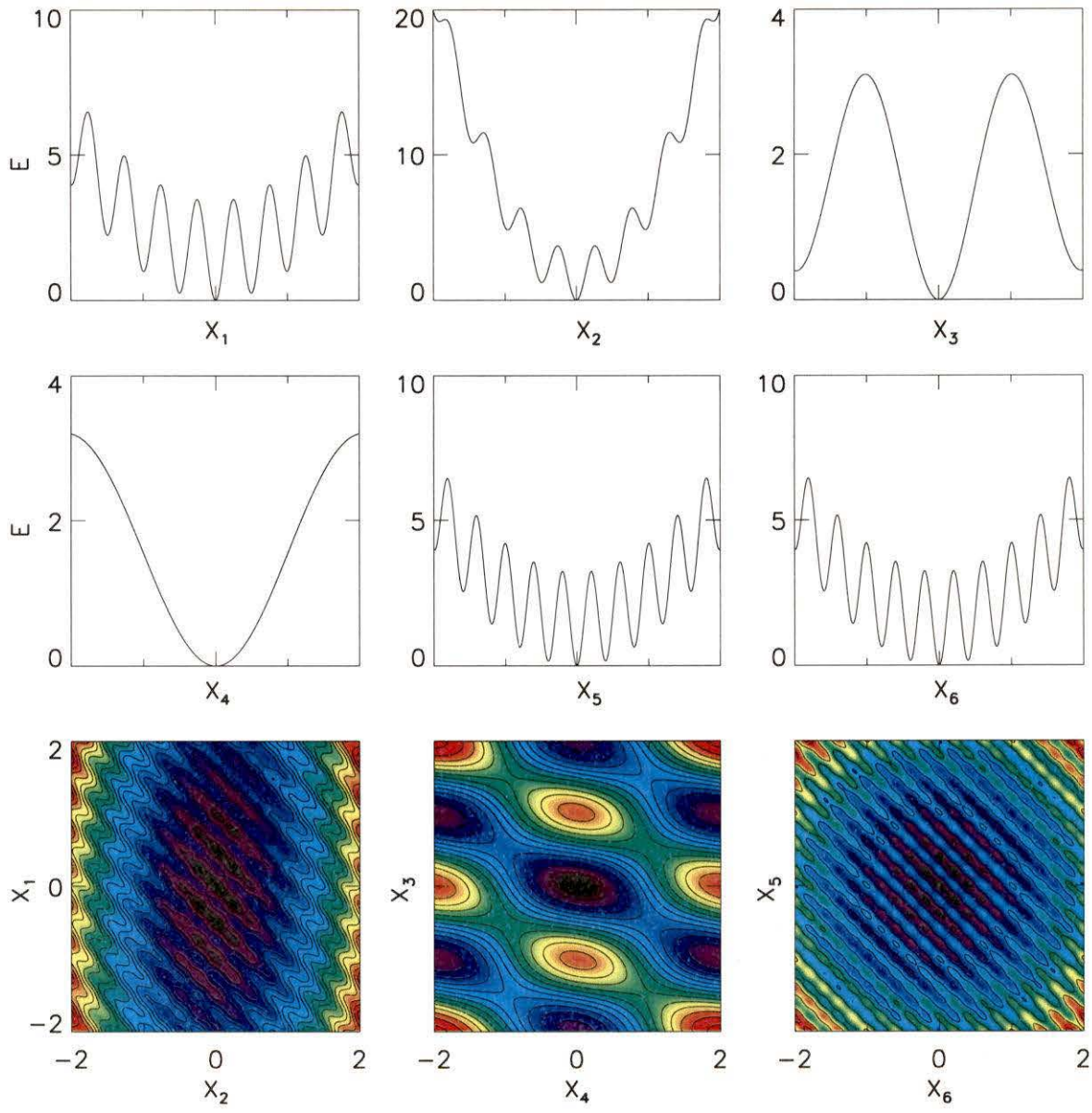

Figure A.1 1-D and 2-D cross sections of the function A.1. In each case the parameters that are not varied are held at their value at the global minimum ($x_i = 0$).

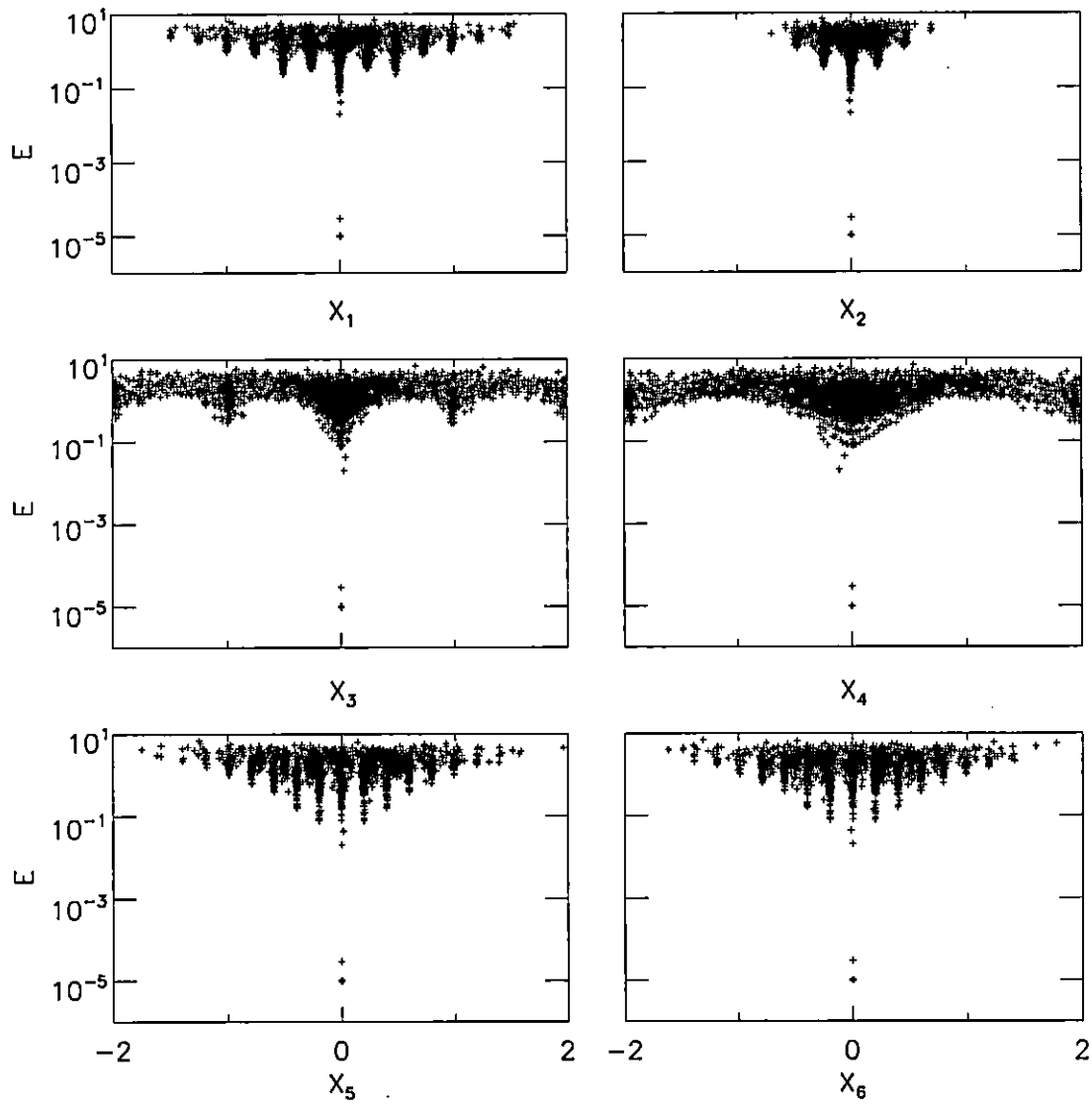

Figure A.2 The results of 5000 independent DHS runs. The point at $E = 10^{-5}$ represents all results that achieved $E \leq 10^{-5}$ (48 results).

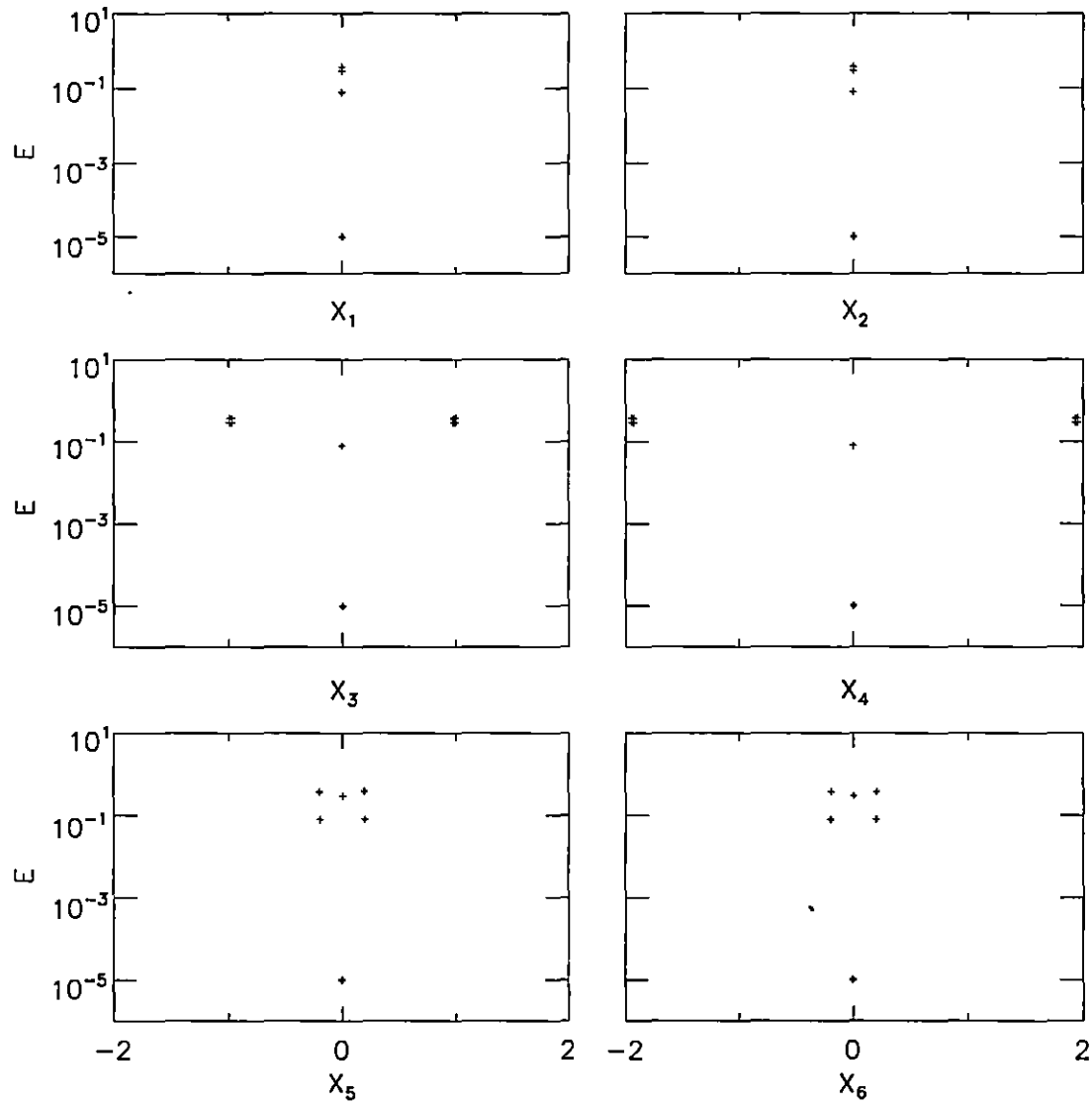

Figure A.3 The results of 100 independent SA runs. The point at $E = 10^{-5}$ represents all results that achieved $E \leq 10^{-5}$ (44 results).

5000 temperature steps, with 10 perturbations per temperature step, and a temperature reduction factor of $\beta = 0.995$. Figure A.3 displays the results of the 100 different runs. In this case, 79% of the parameter values were within $x_i \leq 10^{-3}$ and 44% of the solutions achieved $E \leq 10^{-5}$.

SSA employed a similar annealing schedule to SA except that the inversion only used 4000 temperature (even with similar annealing schedules, SSA required far fewer function evaluations since it perturbs all parameters at once). Figure A.4 displays the results of the 100 different runs. For the SSA runs, 98% of the parameter values were within $x_i \leq 10^{-3}$ and 93% of the solutions achieved $E \leq 10^{-5}$.

The above results indicate that all three methods are capable of good results for a multimodal function. The DHS method frequently became trapped in local minima but did obtain some good results. SA is more effective (although not foolproof) at obtaining the global minimum, but was not particularly effective at moving downhill within this minimum. In this example, SSA achieved solutions deep in the global minimum virtually every time. Of the three methods, SSA also required an order of magnitude fewer function evaluations.

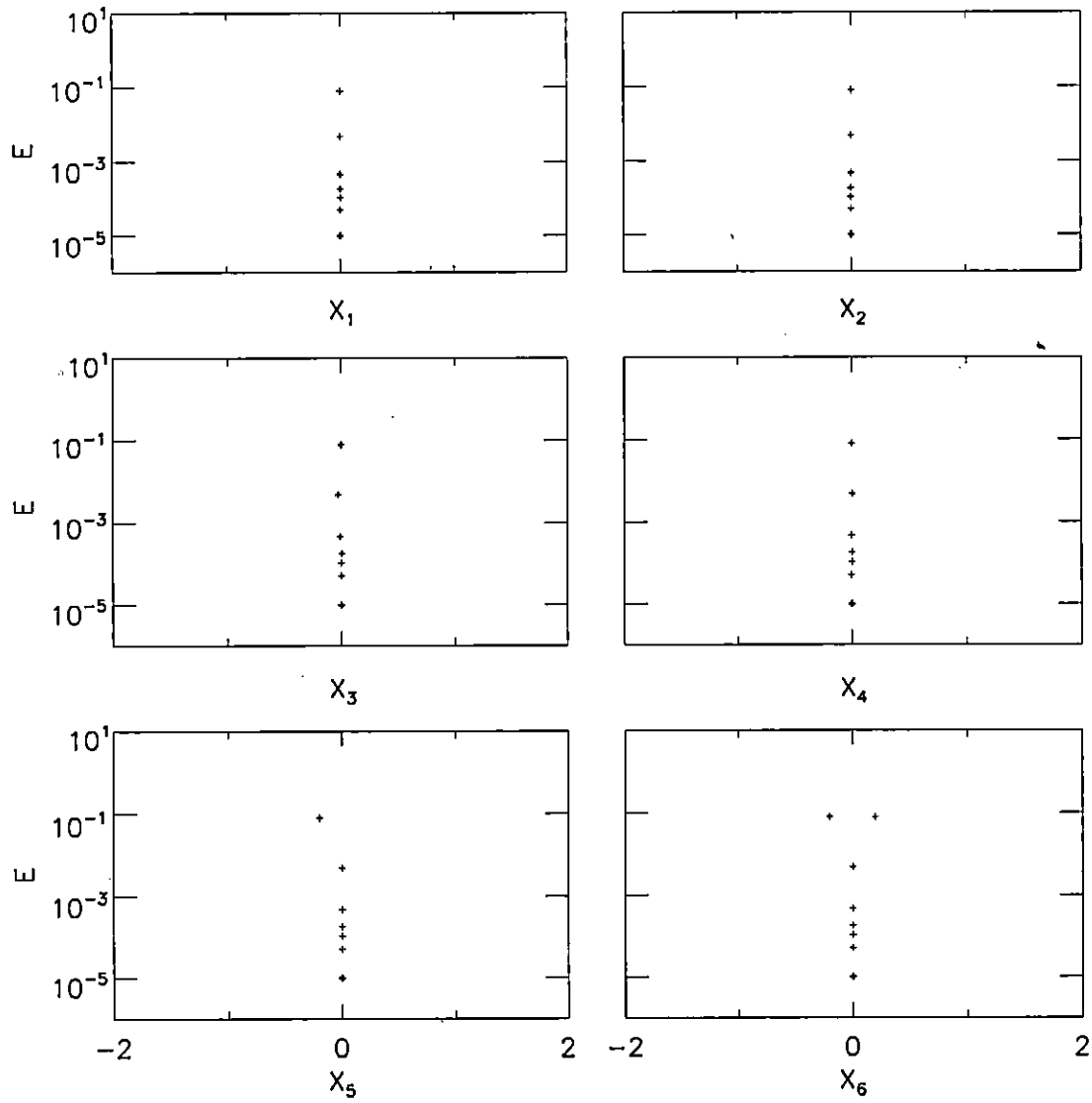

Figure A.4 The results of 100 independent SSA runs. The point at $E = 10^{-5}$ represents all results that achieved $E \leq 10^{-5}$ (93 results).

Appendix B

Forward model input files

B.1 ORCA

Orca SVP input file

```
*(1)   ver_no   SVP title
   1.0   SSA
-------------------------------------------------------------------------------
*(2)   cp   cs   rho   ap   as   for upper halfspace
       343       0   0.00121000       0       0
-------------------------------------------------------------------------------
*(3)   nsvp   ctol
         2       0
-------------------------------------------------------------------------------
*(4)   z   cp
         0    1480       1       0
        117.531    1460
-------------------------------------------------------------------------------
*(5)   nbot
          1
-------------------------------------------------------------------------------
*(6) ii  h  cp1 cp2/g  cs1  cs2  rho1 rho2  ap1 ap2  as1 as2  beta/g ctol
          1      36.1798      1544.08      1649.59       0       0
      1.65990      1.65990    -0.230000    -0.230000       0       0
-------------------------------------------------------------------------------
*(7)   cp   cs   rho   ap   as   for lower halfspace
        1706.07       0      1.80956    -0.230000       0
-------------------------------------------------------------------------------
*(8)   ntop
```

```
        0
-------------------------------------------------------------------------------
*(9) ii  h  cp1 cp2/g  cs1  cs2  rho1 rho2  ap1 ap2  as1 as2  beta/g ctol
-------------------------------------------------------------------------------
```

Orca OPT input file

```
*(1)   ver_no   iicw   iikpl   iirc   n_env
       1.01000      1      0      0      0
-------------------------------------------------------------------------------
*(2)   iirx   cphmin   cphmax   rmin   rmax   phfac   db_cut   iifb   iidiag
        0       0       0       0      0       4       50      0       0
-------------------------------------------------------------------------------
*(3)   nf   f1   f2   ...
        1      100.000
-------------------------------------------------------------------------------
*(4)  iitl  iimf  iisig  iimt  iidc  iikn  iieig  iikrak  iioas  iifepe  iimlab
        1       0       0       0       0       0       1       0       0
      0       0
-------------------------------------------------------------------------------
If iitl=1
*(5)  nzs  zs1  zs2  ...(m)  nzr  zr1  zr2  ...(m)  nr  r1  r2  ...(km)
        1      27.5553    -100       1     100       1      1.25378
-------------------------------------------------------------------------------
*(6)  iir/i  iim/p  nzm  zm1  zm2  ...
        0       1    -100       2    1000
-------------------------------------------------------------------------------
*(7)  fs  nfft/Tw  fmin  fmax  ifft  iiout  iift  iimt  iidc
      200     -2.50000      10      50       1       0       0       0
      0
-------------------------------------------------------------------------------
If iift=1
*(8)  nzs  zs1  zs2  ...(m)  nzr  zr1  zr2  ...(m)  nr  r1  r2  ...(km)
        1     100       1     200     -20    0.0500000      10
```

```
------------------------------------------------------------------------------
*(9)  nrun  npram  [(obt  nlay  ktb  pc  val1  val2),  j=1,npram]
       10       1       0       1       2       0     200     100
------------------------------------------------------------------------------
*(10)  zs  n_src_seg  array_geom_file_name
       20       1nosc_v1
------------------------------------------------------------------------------
      1  iic  v  t1  t2  +dt/-nt  cpa  phi  (POLAR FORM)
*(11)  2  iic  v  t1  t2  +dt/-nt  x1  y1  x2  y2  (X-Y FROM)
        1       0       5       0      60    -100       2      45
------------------------------------------------------------------------------
*(12)  freq  iivar  iikf  kr1  kr2  nkr  ki1  ki2  nki  nduct  iiph  iishp  iishs
       25       1       1     0.800000       1     101     0.100000       0
    101       0       2       1       1
------------------------------------------------------------------------------
*(13)  freq1  freq2  nfreq  iilog  theta1  theta2  ntheta
       10      50      41       0      90       0      91
------------------------------------------------------------------------------
*(14)  freq1  freq2  fs  nfft  theta1  theta2  ntheta
       10      50     100     512      90       0      91
------------------------------------------------------------------------------
```

B.2 PROSIM

Prosim fort.10 input file

```
PROSIM-97 INVERSION
      1
    500
      1        500        500
      0          0
```

```
135.000          0          0          0.500000          0
   0.00000       1520
   10.0000       1517
   50.0000       1515
   135.000       1510
7.00000          1.50000       -0.0600000
   0.00000          1485.00
   7.00000          1485.00
1.80000        -0.150000          1550.00
 0           0
133.400          0          0          1.00000          0
   0.00000       1520
   10.0000       1517
   50.0000       1515
   133.400       1510
7.00000          1.50000       -0.0600000
   0.00000          1485.00
   7.00000          1485.00
1.80000        -0.150000          1550.00
 0           0
131.800          0          0          1.50000          0
   0.00000       1520
   10.0000       1517
   50.0000       1515
   131.800       1510
7.00000          1.50000       -0.0600000
   0.00000          1485.00
   7.00000          1485.00
1.80000        -0.150000          1550.00
 0           0
130.200          0          0          2.00000          0
   0.00000       1520
   10.0000       1517
```

```
      50.0000        1515
      130.200        1510
    7.00000         1.50000      -0.0600000
      0.00000         1485.00
      7.00000         1485.00
    1.80000       -0.150000         1550.00
     0          0
    128.600          0          0          2.50000          0
      0.00000        1520
      10.0000        1517
      50.0000        1515
      128.600        1510
    7.00000         1.50000      -0.0600000
      0.00000         1485.00
      7.00000         1485.00
    1.80000       -0.150000         1550.00
     0          0
    127.000          0          0          10          0
      0.00000        1520
      10.0000        1517
      50.0000        1515
      127.000        1510
    7.00000         1.50000      -0.0600000
      0.00000         1485.00
      7.00000         1485.00
    1.80000       -0.150000         1550.00
     0          0
PULSE
   2048     300     500  -10240
     2.50000          0          1
     26        120         48
     12.0000
     1.00000
```

```
0.978723
0.957447
0.936170
0.914894
0.893617
0.872340
0.851064
0.829787
0.808511
0.787234
0.765957
0.744681
0.723404
0.702128
0.680851
0.659574
0.638298
0.617021
0.595745
0.574468
0.553191
0.531915
0.510638
0.489362
0.468085
0.446809
0.425532
0.404255
0.382979
0.361702
0.340426
0.319149
0.297872
```

```
0.276596
0.255319
0.234043
0.212766
0.191489
0.170213
0.148936
0.127660
0.106383
0.0851064
0.0638298
0.0425532
0.0212766
0.00000
```

Vita

Surname:	Fallat
Given Names:	Mark Ryan
Place of Birth:	Burns Lake, British Columbia, Canada

Educational Institutions Attended:

Camosun College, Victoria, B.C.	1992–1993
University of Victoria, Victoria, B.C.	1993–1999

Diplomas & Degrees Awarded:

Bachelor of Science, UVic	1997

Partial Copyright License

I hereby grant the right to lend my thesis to users of the University of Victoria Library, and to make single copies only for such users or in response to a request from the Library of any other university, or similar institution, on its behalf or for one of its users. I further agree that permission for extensive copying of this thesis for scholarly purposes may be granted by me or a member of the University designated by me. It is understood that copying or publication of this thesis for financial gain shall not be allowed without my written permission.

Title of thesis:

Simplex Simulated Annealing, a Hybrid Approach to Geoacoustic Inversion with Application to Mediterranean Sea Acoustic Data

Author:

Mark Ryan Fallat

March 10, 1999